

1 Vegetation and geochemical responses to Holocene rapid 2 climate change in Sierra Nevada (SE Iberia): The Laguna 3 Hondera record

4 Jose Manuel Mesa-Fernández^{1, 2}, Gonzalo Jiménez-Moreno¹, Marta Rodrigo-Gámiz²,
5 Antonio García-Alix^{1,2}, Francisco J. Jiménez-Espejo³, Francisca Martínez-Ruiz², R.
6 Scott Anderson⁴, Jon Camuera¹ and María J. Ramos-Román¹

7 ¹ Departamento de Estratigrafía y Paleontología, Universidad de Granada (UGR), Avda. Fuente Nueva
8 s/n, 18002, Granada, Spain

9 ² Instituto Andaluz de Ciencias de la Tierra (IACT), CSIC-UGR, Avenida de las Palmeras 4, 18100,
10 Armilla, Granada, Spain

11 ³ Department of Biogeochemistry (JAMSTEC), Yokosuka, Japan.

12 ⁴ School of Earth Sciences and Environmental Sustainability, Northern Arizona University, Flagstaff,
13 AZ, USA.

14 *Correspondance to:* Jose Manuel Mesa-Fernández (jmesa@iact.ugr-csic.es)

15 **Abstract.**

16 High-altitude peat bogs and lacustrine records are very sensitive to climate changes and atmospheric dust
17 input. Recent studies have shown a close relationship between regional climate aridity and enhanced
18 eolian input to lake sediments. However, changes in regional-scale dust fluxes due to climate variability
19 at short-scales and how alpine environments were impacted by climatic- and human-induced
20 environmental changes are not completely understood.

21 Here we present a multi-proxy (palynological, geochemical and magnetic susceptibility) lake sediment
22 record of climate variability in the Sierra Nevada (SE Iberian Peninsula) over the Holocene. Magnetic
23 susceptibility and geochemical proxies obtained from the high mountain lake record of Laguna Hondera
24 evidence humid conditions during the Early Holocene, while a trend towards more arid conditions is
25 recognized since ~7000 cal yr BP, with enhanced Saharan eolian dust deposition until Present. This trend
26 towards enhanced arid conditions was modulated by millennial-scale climate variability. Relative humid
27 conditions occurred during the Iberian Roman Humid Period (2600-1450 cal yr BP) and predominantly
28 arid conditions occurred during the Dark Ages and the Medieval Climate Anomaly (1450-650 cal yr BP).
29 The Little Ice Age (650-150 cal yr BP) is characterized in the LH record by an increase in runoff and a
30 minimum in eolian input. In addition, we further suggest that human impact in the area is noticed through
31 the record of *Olea* cultivation, *Pinus* reforestation and Pb pollution during the Industrial Period (150 cal
32 yr BP-Present). Furthermore, we estimated that the correlation between Zr and Ca concentrations stands
33 for Saharan dust input to the Sierra Nevada lake records. These assumptions support present-day
34 biochemical observations, pointing to eolian input as the main inorganic nutrient source for oligotrophic
35 mountain lakes.

36 **1. Introduction**

37 The southern Iberian Peninsula has been the location for a number of recent studies detailing past
38 vegetation and former climate of the region (Carrión et al., 2001, 2003, 2007, 2010; Carrión, 2002;
39 Combourieu Nebout et al., 2009; Jiménez-Espejo et al., 2008; Martín-Puertas et al., 2008, 2010; Fletcher

40 et al., 2010; Nieto-Moreno et al., 2011, 2015; Rodrigo-Gámiz et al., 2011; Moreno et al., 2012 Jiménez-
41 Moreno et al., 2015). Some of these studies have also documented that the western Mediterranean area
42 has been very sensitive to short-term climatic fluctuations throughout the Holocene (e.g., Fletcher and
43 Sánchez-Goñi, 2008; Combourieu Nebout et al., 2009; Fletcher et al., 2010; Jiménez-Moreno et al.,
44 2013). However, a subset of recent studies have attempted to determine how Mediterranean alpine
45 environments have been affected by Holocene climate change through the study of sedimentary records
46 from high elevation wetlands in the Sierra Nevada (Anderson et al., 2011; García-Alix et al., 2012, 2013;
47 Jiménez-Moreno and Anderson, 2012; Jiménez-Moreno et al., 2013; Jiménez-Espejo et al., 2014; Ramos-
48 Román et al., 2016; García-Alix et al., 2017). These alpine lake and bog records show minimal anthropic
49 influence because they are usually elevational higher than major regional Late Holocene human landscape
50 modification. This allows for a potentially clearer climatic signal to be determined from these sites. Even
51 though human impact is less important at high-elevations, the impacts of human activities has also been
52 reconstructed from these Late Holocene sedimentary records (Anderson et al., 2011; García-Alix et al.,
53 2012, 2013; 2017, 2018).

54 Several studies have highlighted the role of atmospheric mineral dust deposition in marine (Pulido-
55 Villena et al., 2008a) and terrestrial (Morales-Baquero et al., 1999; Ballantyne et al., 2011) ecosystem
56 fertilization through major micronutrients supply. Similar results have been described in the Sierra
57 Nevada alpine lakes, where Saharan dust is especially important in conditioning plankton communities
58 from oligotrophic lakes (Morales-Baquero et al., 2006a, 2006b; Mladenov et al., 2008; Pulido-Villena et
59 al., 2008b; Reche et al., 2009). Although this eolian signal has been occasionally recorded in the
60 sedimentary sequences from the Sierra Nevada lakes (Jimenez-Espejo et al., 2014; García-Alix et al.,
61 2017), the record of inorganic nutrients in Saharan dust input in past lake geochemistry has remained
62 elusive. This study investigates a multiproxy sediment core record from Laguna Hondera (LH), located in
63 the Sierra Nevada range with two main goals: (1) identifying and characterizing climatic variability
64 during the Holocene, focusing on vegetation changes, eolian input and runoff sediments variations; and
65 (2) understanding the Saharan dust influence in past lake sedimentation and geochemistry.

66 **2. Study Area**

67 Sierra Nevada is the highest mountain range in the southern Iberian Peninsula. Bedrock of the high
68 elevations of the Sierra Nevada is mostly composed of metamorphic rocks, principally mica schists
69 (Castillo Martín, 2009). During the late Pleistocene, the Sierra Nevada was one of the southernmost
70 mountains to support alpine glaciers and its last advance was recorded during the Little Ice Age (LIA;
71 Palma et al., 2017; Oliva et al., 2018). Subsequently to the melting of ice at the end of the Last Glacial
72 Maximum, wetlands and small lakes formed in the glacial cirque basins, which occur between 2451 and
73 3227 masl (Schulte, 2002; Castillo Martín, 2009; Palma et al., 2017). Several alpine wetland and lakes
74 have been studied in this area during the last few years as shown in Figure 1.

75 **2.1. Regional Climate and Vegetation**

76 Mediterranean climate characterises southern Iberia, with a marked seasonal variation between warm and
77 dry summers and cool and humid winters (e.g. Lionello et al., 2006). Overprinting this general climate is

78 the influence of the North Atlantic Oscillation (NAO) (Trigo et al., 2004; Trouet et al., 2009). Southern
79 Iberia is also characterized by strong altitudinal contrasts, which in turn control the precipitation patterns,
80 with mean annual values ranging from $<400 \text{ mm yr}^{-1}$ to $>1400 \text{ mm yr}^{-1}$ in the southeast desert lowlands
81 and the southwest highland, respectively (Jiménez-Moreno et al., 2013 and references therein).
82 As with most mountainous regions, species and species groupings in the Sierra Nevada are distributed
83 with respect to elevation, depending on the temperature and rainfall gradients (e.g., El Aallali et al., 1998;
84 Valle, 2003). Above 2800 masl the crioromediterranean flora occurs as tundra-like open grassland. The
85 oromediterranean belt (1900-2800 masl) mostly includes dwarf *Juniperus* (juniper) xerophytic shrublands
86 and pasturelands and *Pinus sylvestris* and *P. nigra*. The supramediterranean belt (~1400-1900 masl) is
87 characterized by mixed deciduous and evergreen forest species (i.e., evergreen and deciduous *Quercus*,
88 with *Pinus spp.* and others). Mesomediterranean vegetation (600-1400 masl) includes sclerophyllous
89 shrublands and evergreen *Quercus* woodlands. The natural vegetation has been strongly altered by human
90 activities and cultivation in the last centuries, increasing significantly the abundance of *Olea* (olive), due
91 to cultivation at lower altitudes (Anderson et al., 2011, and references therein), and *Pinus* due to
92 reforestation primarily at higher elevations (Valbuena-Carabaña, 2010).

93 **2.2. Laguna Hondera**

94 Laguna Hondera (hereafter LH; 2899 masl; 37°02.88'N, 3°17.66'W, lake surface: 0.0053 km²; maximum
95 depth: 0.8 m; Morales-Baquero et al., 1999; Fig. 1) is a small and shallow lake located at the lowest
96 elevation of a set of lakes locally named Cañada de Siete Lagunas, a glacial valley between two of the
97 highest peaks of the mountain range in the Iberian Peninsula: Alcazaba (3366 masl) and Mulhacén (3479
98 masl). LH has a catchment area of 1.546 km², which is much larger than previously studied sites in the
99 region (Laguna de Río Seco, LdRS, 0.099 km²; Borreguil de la Caldera, BdIC, 0.62 km²; Morales-
100 Baquero et al., 1999; Ramos-Román et al., 2016; Fig 1 for locations). The lake was reduced to a little
101 pond in the deepest area of the basin when cored in September 2012, with a maximum depth of only a
102 few centimetres.
103 LH presently occurs in the crioromediterranean vegetation belt (2800 masl) (El Aallali et al., 1998; Valle
104 et al., 2003). The bedrock in the LH basin consists in Paleozoic and Precambrian mica schist with
105 disthene and staurolite of the lower part of the Caldera Formation (Díaz de Federico et al., 1980).

106 **3. Methods**

107 **3.1. Core sampling, lithology and chronology**

108 Six sediment cores were recovered from LH with a Livingstone piston corer in September 2012. LH 12-
109 03 (83 cm) was selected for a multi-proxy study because it was the longest core. Cores were wrapped
110 with tin foil and plastic film and transported to Universidad de Granada, where they were stored at 4°C.
111 Core LH 12-03 was split longitudinally and the sediments were described. Magnetic susceptibility was
112 measured every 0.5 cm with a Bartington MS2E in SI units ($\times 10^{-4}$) (Fig. 2). The sediment cores were
113 subsampled every 1 cm for several analyses, including pollen and geochemistry.

114 The age model was built using seven AMS radiocarbon dates from vegetal remains (Table 1; Fig. 2) by
115 means of Clam software (Blaauw, 2010; version 2.2), which used the IntCal13 curve for radiocarbon age
116 calibration (Reimer et al., 2013). A smooth spline approach was chosen (Fig. 2). The sediment
117 accumulation rate (SAR) was calculated with the average rate from the Clam smooth spline output (Fig.
118 2).

119 3.2. Pollen

120 Pollen analysis was performed on 1 cm³ of sample collected at regular 1 cm interval throughout the first
121 62 cm of the core. Older sediments (from 62 to 82 cm depth) were barren in pollen, and only one interval
122 at 73 cm could be studied (Fig. 2). Pollen extraction included HCl and HF treatment, sieving, and the
123 addition of Lycopodium spores for calculation of pollen concentration (modified from Faegri and Iversen,
124 1989). Sieving was done using a 10 µm nylon sieve. The resulting pollen residue was suspended in
125 glycerine and mounted on microscope slides. Slides were analysed at 400x magnification counting a
126 minimum of 300 pollen grains, not including the local aquatic species Cyperaceae, Ranunculaceae
127 and *Typha*. An overview of pollen taxa with abundances >1% for core LH 12-03 is plotted using the Tilia
128 software (Grimm, 1993) in Figure 3. The pollen zonation was delimited visually by a cluster analysis
129 constrained by age of taxa abundance >1% using CONISS software (Grimm, 1987) (Fig. 3). *Olea* were
130 differentiated from others Oleaceae, such as *Phillyrea*, based on the thicker intine and higher size of
131 reticulum in polar vision (Beug, 2004).

132 3.3. Geochemical analyses

133 X-ray fluorescence (XRF) Avaatech core scanner®, located at the University of Barcelona, was used to
134 measure light and heavy elements in the LH 12-03 core. An X-ray current of 650 µA, a 10 second count
135 time and 10 kV X-ray voltage was used for measuring light elements, whereas 1700 µA X-ray current, 35
136 second count time and 30 kV X-ray voltage was used for heavy elements. Sampling interval for these
137 analyses was every 0.5 cm. For our study only three elements (K, Ca and Ti) have been considered with
138 enough counts to be representative.

139 Inductively coupled plasma-optical emission spectrometry (ICP-OES; Perkin-Elmer optima 8300) was
140 used for major element analysis measurements on discrete samples every 2 cm. Prior to analysis, the
141 samples were dried in an oven and digested with HNO₃ and HF. Blanks and international standards were
142 used for quality control, the analytical accuracy was higher than ± 2.79% and 1.89% for 50 ppm
143 elemental concentrations of Al and Ca, respectively, and better than ± 0.44% for 5 ppm elemental
144 concentrations of K.

145 Trace element analysis was performed with an inductively coupled plasma mass spectrometry (ICP-MS;
146 Perkin Elmer Sciex Elan 5000). Samples were measured in triplicate through spectrometry using Re and
147 Rh as internal standards. The instrumental error is 2% for elemental concentrations of 50 ppm (Bea,
148 1996). Both ICP-OES and ICP-MS analyses were performed at the Centre for Scientific Instrumentation
149 (CIC), University of Granada, Spain.

150 3.4. Mineralogical analyses

151 Morphological and compositional analyses were performed using scanning electron microscopy (SEM)
152 with an AURIGA model microscope (Carl Zeiss SMT) coupled with energy-dispersive X-ray
153 microanalysis (EDX) and Electron Backscatter Diffraction (EBSD) mode, also at the CIC (University of
154 Granada, Spain). Mineral grains were analysed to determine provenance, in particular those from eolian
155 origin.

156 **3.5 Statistical Analysis**

157 R-mode principal components analysis (PCA) was run on the geochemical dataset using the PAST
158 software (Hammer et al., 2001). PCA identifies hypothetical variables (components) accounting for as
159 much as possible of the variance in multivariate data (Davis, 1986; Harper, 1999). The elements used in
160 the PCA were standardized by subtracting the mean and dividing by the standard deviation (Davis, 1986).
161 Pb was not included in the PCA analysis due to its anthropogenic origin from mining and industrial
162 pollution during the latest Holocene in this area (García-Alix et al., 2013).

163 **4. Results**

164 **4.1. Lithology and magnetic susceptibility**

165 The LH 12-03 sediment core consists primarily of peat in the upper ~60 cm, with mostly sand and clay
166 layers below (Fig. 2). Positive MS peaks coincide with the grey clay intervals between 58 and 72 cm. Peat
167 intervals coincide with relatively low MS values. For example, a minimum in MS occurs at 36-48 cm
168 depth, related with a peaty interval with root remains. Near the bottom of the core, between 76 and 80 cm,
169 a sandy oxidized interval occurs.

170 **4.2. Chronology and sedimentation rate**

171 The age model of LH 12-03 documents that the record spans the last 10800 cal yr BP (Table 1; Fig. 2).
172 Sediment accumulation rates (SAR) were calculated using the average rate from the Clam smooth spline
173 output (Fig. 2). The SAR below ~39 cm is very constant, varying between 0.049 and 0.061 mm yr⁻¹. The
174 SAR increases exponentially to 0.098 mm yr⁻¹ at 22 cm, 0.167 mm yr⁻¹ at ~9 cm and 0.357 mm yr⁻¹ at
175 the core top. Accordingly with the model age and the SAR, resolution of pollen analysis varies between
176 ~40 years per sample in the top of the core and ~120 years per sample in the lower part. The resolution of
177 the geochemical analysis on discrete samples changes between 100 and 400 years per sample, but the
178 geochemical XRF core scanning resolution ranges between 15 and 100 years per sample, providing
179 higher resolution than geochemical data on discrete sample. The MS analyses resolution varies between
180 15 and 100 years per sample.

181 **4.3. Pollen**

182 Fifty distinct pollen taxa were recognized, but only those with abundance higher than 1% are included in
183 the pollen diagram (Fig. 3). Four pollen zones for the LH 12-03 record are identified, using variation in
184 pollen species plotted in Figure 3 and a cluster analysis run through the CONISS software (Grimm,
185 1987).

186 Zone LH-1 (core bottom-2600 cal yr BP) is subdivided in two subzones. Subzone LH-1A (bottom-4000
187 cal yr BP) is defined by the alternation between Arboreal Pollen (AP) and herbs. AP is composed
188 primarily of *Pinus*, but also *Quercus*. During the interval from ~9500 to ~7000 cal yr, BP only three
189 samples were analysed, due to the low preservation of pollen in this interval. Pollen in this period is
190 dominated by an alternation between Asteraceae (3-60%) and *Pinus* (5-90%) (Fig. 3). The highest
191 occurrence of Onagraceae (~10%) is identified in this subzone, and Caryophyllaceae reach high values
192 (~10%) as well. Only minor amounts of graminoids (Poaceae and Cyperaceae) occur during this period.
193 Between ~7000 to ~4000, *Pinus* pollen decreases from 90 % to ~55%, with a minimum (~30%) at 5000
194 cal yr BP. *Quercus* increase from ~2% to ~10%. The highest percentages of *Betula* (~5%) in the record
195 occurs at this time. Asteraceae pollen decreases (~5-30%), but Poaceae increase from <5% to >25%.
196 Cyperaceae occur in high percentages (15%).
197 The subzone LH-1B (~4000-2600 cal yr BP) is defined primarily by a great increase in Poaceae pollen (to
198 ~60%) (Fig. 3). Other important herbs and shrubs include Asteraceae (5-15%) and Caryophyllaceae
199 (~5%). Other pollen types that increase for the first time in this zone include Ericaceae (~3%), *Artemisia*
200 (~3%) and Ranunculaceae (~2-6%). *Pinus* (~3-25%) and Cyperaceae (0-14%) record a minimum in this
201 zone, and Onagraceae disappear altogether (Fig. 3).
202 Zone LH-2 (~2600-1450 cal yr BP) pollen assemblages show high variability. *Pinus* pollen variates
203 between ~80% to ~3% from the onset to the end of the zone. Aquatic pollen such as Cyperaceae (~15%)
204 increases. On the other hand, an increase in herbs such as Asteraceae (~5-70%) occurs along the zone,
205 Poaceae pollen variates between ~7 and 12%.
206 Zone LH-3 (~1450-150 cal yr BP) is subdivided in two subzones. Subzone 3A (~1450-600 cal yr BP) is
207 characterized by an increase in herbaceous pollen, led by Poaceae (~35% maximum during this zone),
208 Asteraceae (~60% maximum during this zone after ~1000 cal yr BP) and *Artemisia* (~10%), with the
209 resulting decrease in AP. Since this subzone to the Present, *Quercus* pollen is the major component of AP
210 instead of *Pinus*. Cyperaceae also show a decrease, and Ranunculaceae reach ~ 5%. Subzone 3B (~600-
211 150 cal yr BP) documents an increase in *Olea* (~6%), Poaceae (20%), Caryophyllaceae (7%) and
212 *Artemisia* (~2-20%). *Pinus* (~2%) and Asteraceae (~20%) decrease in this period. Aquatic and wetland
213 pollen show a rise (Cyperaceae ~30%, Rannunculaceae ~10%).
214 Zone LH-4 (~ 150 cal yr BP-Present) depicts a further increase in *Olea* (~25%), Poaceae (~40%) and
215 *Artemisia* (~10%).

216 4.4. Sediment composition

217 The XRF-scanning method relies on determining the relative variations on elements composition.
218 Nevertheless, due to the presence of major variations in organic matter or carbonates it is necessary to
219 normalize the measured count in order to obtain an environmentally relevant signal (Löwemark et al.,
220 2011). Aluminium and titanium normalizations are commonly used to discern possible fluctuations in the
221 lithogenic fraction (enrichment or depletion of specific elements), particularly in the terrigenous
222 aluminosilicate sediment fraction (Van der Weijden, 2002; Calvert and Pedersen 2007; Martinez-Ruiz et al.
223 et al., 2015). For this study, the XRF data were normalized to Ti since Al counts obtained were very low.
224 Poor detection of Al can be related to either low Al content, or high organic and water contents that

225 increase radiation absorption and affect the intensity of this light element, among other possibilities (e.g.
226 Tjallingii et al., 2007).

227 Since data spacing is different between the analyses on discrete samples and the XRF scanner, a linear
228 interpolation was performed with the purpose of equalizing the space of the different time series (150-300
229 years). Afterwards, the mobile average was worked out along the time series (taking into account the five
230 nearest points) in order to easily identify trends by means of smoothing out data irregularities. The
231 obtained data were compared, and both XRF-scanner and discrete sample data showed a good correlation.
232 Consequently, the geochemical proxies displayed higher time resolution than the discrete samples (Table
233 2). Discrete sample and XRF data results are described together in order to simplify this section (Fig. 4).

234 The lower part of the core is typified by maximum values of K/Al and K/Ti ratios, coinciding with the
235 lowest values in Ca/Al, Ca/Ti and Zr/Al ratios. Pb/Al data show a stable pattern during this interval.
236 Nevertheless, between 10000 and 9000 cal yr BP and ~8200 cal yr BP the trends were reversed, with
237 relatively low K/Al, low K/Ti and slightly increasing Zr/Al, Ca/Al and Ca/Ti ratios. A positive peak in
238 Pb/Al ratio at ~8200 cal yr BP is also observed.

239 Between ~7000 and 4000 cal yr BP a decreasing trend in K/Al and K/Ti ratios occurs along with an
240 increasing trend in Zr/Al, Ca/Al and Ca/Ti ratios. The Pb/Al ratio remains constant throughout this
241 interval.

242 From ~4000 to ~2600 cal yr BP an increase in Zr/Al, Ca/Al and Ca/Ti ratios is documented. A maximum
243 in these proxies occurs at ~2600 cal yr BP. A K/Al and K/Ti minima occurs between ~3000 and ~2600
244 cal yr BP. The Pb/Al ratio shows a positive peak at ~2800 cal yr BP.

245 The interval between ~2600 and ~1450 cal yr BP is characterized by low Ca/Al, Ca/Ti and Zr/Al ratios,
246 with relatively high K/Al and K/Ti ratios. The Pb/Al ratio shows a flat pattern, increasing at ~1500 cal yr
247 BP.

248 The period between ~1450 and ~650 cal yr BP depicts higher ratios of Zr/Al, Ca/Al and Ca/Ti and
249 decreasing ratios of K/Al and K/Ti. A somewhat higher Pb/Al ratio is also registered during this interval.

250 From ~650 to ~150 low values of Zr/Al and Ca/Ti ratios and minimum values Ca/Al ratio occur. Higher
251 K/Al and K/Ti values are also observed. The Pb/Al ratio decreases during this interval. From ~150 to the
252 Present, an increase in Zr/Al, Ca/Al, Ca/Ti, K/Ti and a Pb/Al maximum occur. Lower K/Al ratio is
253 recorded during this period.

254 Several studies have demonstrated that PCA analysis of geochemical data can elucidate the importance of
255 different geochemical components driving the environmental responses in marine and lacustrine records
256 (Bahr et al., 2014; Yuan, 2017). We performed a PCA analysis of the LH geochemical data, which
257 yielded two significant components (Fig. 5). The first principal component (PC1) describes 58% of the
258 total variance. The main negative loadings for PC1 are Rb, Ba, Al, K, Ca, Mg and Sr, while large positive
259 loadings correspond to Zr and Rare Earth Elements (REE). The second principal component (PC2)
260 explains 17% of the total variance. The main negative loading for PC2 are Fe, Ca, Zr, Mg and Lu.
261 Positive loads correspond to Al, K, Ba, Sr and other elements.

262 SEM analyses show an alternation between a lithology rich in rock fragments and another rich in organic
263 remains. Also, diatom frustules, rich in silica, are particularly abundant since ~6300 cal yr BP to Present.
264 Other minerals such as zircon, rounded quartz and monazite were also identified (Fig. 6).

265 5. Discussion

266 Pollen and geochemical proxies have been widely used for reconstructing vegetation changes and
267 environmental and climate variations in southern Iberia (e.g. Carrión, 2002; Sánchez-Goñi and Fletcher,
268 2008; Anderson et al., 2011; Nieto-Moreno et al., 2011; Jiménez-Moreno and Anderson, 2012; Moreno et
269 al., 2012; Fletcher and Zielhofer, 2013; Jiménez-Espejo et al., 2014; Ramos-Román et al., 2016).
270 Variations in the occurrences of arboreal taxa such as *Pinus* and other mesic species (e.g. *Betula*,
271 *Quercus*), indicating relative humid and warm conditions, and xerophytic species (e.g., Poaceae,
272 Asteraceae, Amaranthaceae, *Artemisia*), representing aridity, have been useful for reconstructing relative
273 humidity changes in southern Iberian (e.g. Carrión et al., 2001, 2007, 2010; Anderson et al., 2011;
274 Jiménez-Moreno and Anderson, 2012; Jiménez-Moreno et al., 2013, 2015; Ramos-Román et al., 2016,
275 2018a, 2018b). *Pinus* reach percentages over 80% in our record. This bisaccate pollen grain is favoured
276 by wind transport and has a larger dispersal area than other tree species, and sometimes might be
277 overrepresented (Poska and Pidek, 2010; Pérez-Díaz et al., 2016). Nevertheless, LH is located at 2899
278 masl only 99 m above treeline and the upper boundary of the oromediterranean belt (1900-2800 masl)
279 where *Pinus sylvestris* is the main tree specie (El Aallali et al., 1998; Valle, 2003). Therefore, this
280 apparently anomalous high concentration of *Pinus* may be caused by an upward migration of the
281 oromediterranean belt and treeline towards higher elevations and around the LH during warmer and more
282 humid periods, which could have been overstated due to its high pollen-production and dispersal.
283 Therefore, *Pinus* seems to be mostly recording a regional climatic signal, without allocthonous influence.
284 Over 75% of the total geochemical data variance is explained by the PC1 and PC2 (Fig. 5). We interpret
285 the results of PC1 as resulting from certain sorting between heavy minerals (positive loading; Zr and
286 REE) vs. clay minerals and feldspars (negative loadings; K, Al and Ca). The drainage basin is composed
287 mainly by mica schist, consequently enhanced in K-rich minerals such as mica and feldspar (Díaz de
288 Federico et al., 1980). This sorting between heavy minerals (enriched in Zr and REE) and clays and
289 feldspars (enriched in K and Al) (Fig. 5a), was probably linked to physical weathering within the basin
290 and to resulting runoff until final deposition in the lake.

291 On the other hand, we interpret the results of PC2 as differentiating autochthonous elements (positive
292 loadings) vs. Saharan allocthonous input (negative loadings). In the first case, due to the abundance of
293 mica schist within the LH drainage basin (Díaz de Federico et al., 1980), the K/Al and K/Ti ratios are
294 interpreted as detrital products, and thus a proxy of runoff. In the second case, PC2 negative loading Zr,
295 Ca, Mg and Fe (Fig. 5b) grouped elements that are coherent with Saharan input composition (dolomite,
296 iron oxides and heavy minerals) (Ávila, 1997; Morales-Baquero et al., 2006b; Moreno et al., 2006;
297 Pulido-Villena et al., 2007). In addition, Ca shows a strong positive correlation with Zr since 6300 cal yr
298 BP ($r = 0.57$; $p < 0.05$) supporting an eolian origin of the Ca in LH sediments. Although we cannot exclude
299 others nearby Ca sources or changes in the source of African dust (Moreno et al., 2006), the 85% of dust
300 reaching south Iberia derives from the Sahara (Morales-Baquero and Pérez-Martínez, 2016; Jiménez et
301 al., 2018). For instance, enrichment in heavy minerals such as zircon and palygorskite has previously
302 been used as an eolian proxy in the western Mediterranean (e.g., Combourieu Nebout et al., 2002,
303 Rodrigo-Gámiz et al., 2011, 2015). High concentrations of Ca in other lacustrine systems are usually
304 associated with biogenic sources when anti-correlated with terrigenous elements (Yuan, 2017).

305 Nevertheless, elevated Ca in the LH record is linked with detrital elements, as shown by PC1, where Ca is
306 associated with K and Al (Fig. 5a). Therefore Ca/Al and Ca/Ti ratios are used in the LH record as Saharan
307 eolian input proxies.

308 Elemental ratio variations, such as the ratios K/Al and K/Ti indicating fluvial input and the ratios Zr/Al or
309 Zr/Th indicating aridity and eolian input, have been previously interpreted in Alboran Sea marine records
310 as well as in southern Iberia lake records (Martín-Puertas et al., 2010; Nieto-Moreno et al., 2011, 2015;
311 Rodrigo-Gámiz et al., 2011; Jiménez-Espejo et al., 2014; Martínez-Ruiz et al., 2015; García-Alix et al.,
312 2017, 2018). Thus, the integration of both palynological data and geochemical ratios used as detrital input
313 from LH have allowed the reconstruction of the palaeoclimate and palaeoenvironmental history in Sierra
314 Nevada during the Holocene.

315 **5.1. Holocene palaeoclimate and palaeoenvironmental history**

316 **5.1.1. Early and Mid-Holocene humid conditions (10800–7000 cal yr BP)**

317 The wettest conditions are recorded during the Early Holocene in Sierra Nevada. This is shown in the LH
318 record by the highest K/Al ratio and MS values, and the low values in Zr/Al, Ca/Al and Ca/Ti ratios,
319 suggesting that runoff dominated over eolian processes at this time (zone LH-1; Fig. 7) and agrees with
320 previous studies in the area (Anderson et al., 2011; Jiménez-Moreno and Anderson, 2012; García-Alix et
321 al., 2012; Jiménez-Espejo et al., 2014). Unfortunately, the pollen record from LH during this interval is
322 insufficient to confirm this interpretation, due to the high detrital sediment composition and low organic
323 content, as shown by the low MS values and low pollen preservation. However, high percentages of AP
324 in two out of three analysed samples suggest humid conditions and high runoff during this period, and
325 maybe an upward migration of the oromediterranean belt inferred by the high *Pinus* percentages.

326 An Early Holocene humid stage is noticed in other nearby sites, such as the south-faced Laguna de Río
327 Seco (LdRS; Fig. 1) (Anderson et al., 2011), when the highest lake level of the Holocene occurred. This is
328 also coeval with the dominance of arboreal species such as *Pinus* as well as aquatic and wetland plants
329 (Anderson et al., 2011). Low eolian input, noted by geochemical ratios, is also recorded in LdRS during
330 this interval (Jiménez-Espejo et al., 2014). Further indications of elevated humidity come from the north-
331 facing Borreguil de la Virgen (BdIV) (see Fig. 1), which is dominated by an AP assemblage and a high
332 occurrence of aquatic algae *Pediastrum* along with a higher lake level (Jiménez-Moreno and Anderson,
333 2012).

334 Although the preponderance of evidence accumulated for the Early Holocene suggests overall humid
335 conditions, at least three relatively arid periods are identified with the geochemical data in the LH record
336 (Fig. 7). The first arid period occurred between ~9600 and 9000 cal yr BP, the second occurred ~8200 cal
337 yr BP and the third around 7500 cal yr BP.

338 The first arid event is characterized in LH by a decrease in K/Al and K/Ti ratios and MS, resulting from
339 the lower runoff input with the concomitant change to a more peaty composition. This event could be
340 correlated with a dryness event recorded in the Siles Lake record (Carrion, 2002) at ~9300 cal yr BP
341 noticed by an increase in *Pseudoschizaea*, which was coeval with a minor decrease in arboreal pollen also
342 recorded in several sites in North Iberia (Iriarte-Chiapusso et al., 2016). At marine site ODP 976 (Fig.1;
343 Combourieu-Nebout et al., 2009) a decrease in deciduous *Quercus* occurred between 9500 and 9200 cal

344 yr BP indicating a rapid excursion towards arid conditions (Fig.7). The speleothem record of Corchia
345 Cave also shows dryer conditions during this interval (Fig. 7; Regattieri et al., 2014) In addition, a
346 decrease in fluvial input in the Southern Alps and an aridification phase in southeastern France and
347 southeastern Iberia has been similarly recorded (Jalut et al., 2000).

348 The second dry event recorded at ~8200 cal yr BP is depicted in LH record by a negative peak in K/Ti
349 and K/Al ratios, and by the onset of a trend toward peatier lithology as evidenced by the MS profile. This
350 event is not recognized in LH record as clearly as the 9500 cal yr BP and the 7500 cal yr BP dry events. A
351 decrease in *Pinus* percentage is observed in the nearby LdRS (Anderson et al., 2011), while a forest
352 decrease is recorded in the Alboran Sea sites MD95-2043 and ODP 976. In several records from north
353 western Iberia, a decrease in arboreal pollen also occurred at this time (Iriarte-Chiapusso et al., 2016).

354 The 8.2 ka event was the most rapid climate change towards cooler conditions occurred during the
355 Holocene. It was defined in Greenland ice cores by minimum values in $\delta^{18}O$ and affected the North
356 Atlantic basin and the Mediterranean area (Alley et al., 1997; Rasmussen et al., 2007; Wiersma et al.,
357 2011). Recent simulations point to a fresh water input in North Atlantic which could slow down the North
358 Atlantic Deep Water (NADW) formation preventing the heat transport over the north hemisphere
359 (Wiersma et al., 2010, 2011; Young et al., 2013).

360 Another dry event is recorded in LH at ~7500 cal yr BP evidenced by the higher peat content in the
361 sediment, as well as by the lower MS values and a relative minimum in the K/Ti ratio. A relative AP
362 minimum also occurred in LH at this time. This short-live event is depicted sharper than 8200 cal yr BP
363 event in several sites in southern Iberia and Alboran Sea: In the Padul record, located at 725 masl at the
364 lower part of Sierra Nevada a decrease in both evergreen and deciduous *Quercus* is interpreted as a dry
365 and cold event (Ramos-Román, 2018; Ramos-Román et al., 2018a); forest expansion in Guadiana valley
366 during the early-mid Holocene is interrupted by a xeric shrublands development between 7850 and 7390
367 cal yr BP (Fletcher et al., 2007); in the Alboran Sea a decrease in deciduous *Quercus* is registered at site
368 MD95-2043; at site 300G a decrease in winter and summer temperatures is also recorded during this
369 interval (Jiménez-Espejo et al., 2008); in lake Pergusa (south Italy) a trend toward arid conditions began
370 at ~7500 cal yr BP (Magny et al., 2012); in Corchia Cave an arid excursion occurred at ~7500 cal yr BP
371 within an overall humid period between 8300 cal yr BP and 7200 cal yr BP (Fig. 7; Regattieri et al.,
372 2014).

373 Importantly, these arid events recorded in LH at 9600 to 9000 cal yr BP and 8200 cal yr BP are coeval
374 with the ice-rafted debris events 6 and 5 defined by Bond et al. (1997) in North Atlantic.

375 **5.1.2. Mid- and Late Holocene (~7000 cal yr BP-2600 cal yr BP)**

376 The Middle and Late Holocene in the southern Iberian Peninsula is characterized by a trend towards more
377 arid conditions (Jalut et al., 2009; Anderson et al., 2011; Rodrigo-Gámiz et al., 2011; Jiménez-Moreno
378 and Anderson, 2012; Jiménez-Espejo et al., 2014). In the LH record an abrupt decrease in the MS values
379 indicates a lithological change to more peaty sedimentation at ~7000 cal yr BP. Similarly, a decrease in
380 the K/Al and K/Ti ratios, points to a transition to less humidity and runoff (Fig. 7). *Quercus* percentage
381 increases at this time, partially replacing the *Pinus*, which mainly compose the AP during the record. A
382 progressive increasing trend in eolian input from Sahara (Zr/Al , Ca/Al and Ca/Ti ratios) is observed

383 around 5500-6500 cal yr BP (Fig. 7), also pointing to an increase in aridity in the area. This change
384 coincides with regional increases in the Zr/Th ratio (equivalent to Zr/Al ratio) and *Artemisia* pollen, and
385 with decreases in *Betula* and *Pinus* in the LdRS record (Anderson et al., 2011; Jiménez-Espejo et al.,
386 2014), and in *Pinus* in the BdlV record (Jiménez-Moreno and Anderson, 2012). Rodrigo-Gámiz et al.
387 (2011) and Jiménez-Espejo et al. (2014) observed similar geochemical patterns in western Mediterranean
388 marine records and in LdRS, with a decline in fluvial input, and a decline in surface runoff, respectively.
389 The same pattern is noticed in marine pollen records MD95-2043 and ODP 976 (Fletcher and Sanchez-
390 Goñi, 2008; Combourieu-Nebout et al., 2009; Fig. 7). Contemporaneously, aridity is also suggested from
391 speleothem data around the Mediterranean area: At El Refugio cave, a hiatus in the speleothem growing
392 rate occurred between 7300 and 6100 cal year BP (Walczak et al., 2015), which is coeval with a drop in
393 $\delta^{18}\text{O}$ in Soreq (Israel) and Corchia (Italy; CC26; Fig. 1 and 7) caves at 7000 cal yr BP (Bar-Matthews et
394 al., 2000; Zanchetta et al., 2007; Regattieri et al., 2014). Also at ~7000 cal yr BP a decreasing trend in the
395 deciduous/sclerophyllous pollen ratio occurred in southeastern France and Iberia (Jalut et al., 2000) and at
396 continental sites around the Mediterranean Sea (Jalut et al., 2009). In addition, very low lake levels were
397 recorded in the Sahara-Sahel Belt (Liu et al., 2007) and in the Southern Alps (Magny et al., 2002).
398 Enhanced arid conditions are observed in the LH record between 4000 and 2500 cal yr BP, interpreted
399 through a decline in AP and a Poaceae maximum. Also a surface runoff minimum and an increase in
400 eolian input proxies took place between 3500 and 2500 cal yr BP (zone LH-3). In Corchia Cave an arid
401 interval was recorded at ~3100 cal yr BP (Regattieri et al., 2014), coeval with another one observed
402 globally and described by Mayewski et al. (2004) between 3500 and 2500 cal yr BP. Nevertheless, this
403 period is not climatically stable, fluctuations are observed in K/Ti, K/Al, Ca/Ti, Ca/Al and Zr/Al ratios.
404 Furthermore, peaks in *Quercus* are recorded in LH, LdlM and ODP 976 sites at ~3900 cal yr BP and
405 ~3100 cal yr BP, when AP in LH decreases (Combourieu-Nebout et al., 2009; Jiménez-Moreno et al.,
406 2013). This fact a priori contradictory, could be explained by altitudinal displacements of the tree taxa
407 such as *Quercus* in the oromediterranean belt due to the climatic variability occurred along this interval
408 (Carrión, 2002). During warmer periods, this species would be displaced towards higher elevation and the
409 influence of *Quercus* pollen in Sierra Nevada would be larger, this could explain relative
410 higher *Quercus* percentages in LdlM, LH and also in the ODP 976 record. The same relationship
411 between *Quercus* and *Pinus* is observed comparing the BdlC and Padul records, located closely but with
412 large altitude difference (BdlC ~2992 masl; Padul ~725 masl; Ramos-Román, 2018) where is also likely
413 linked to movements in the oromediterranean belt (Ramos-Román, 2018). These altitudinal displacements
414 of the tree taxa have been previously related to temperature changes in others southern Iberian records,
415 suggesting an ecological niche competition between *Pinus* and *Quercus* species at middle altitudes (see
416 Carrión et al., 2002 for a revision).

417 **5.1.3. Iberian Roman Humid Period (IRHP; ~2600-1450 cal yr BP)**

418 Because there is no consensus in the literature about the chronology for the main climatic stages during
419 the last 2000 years (Muñoz-Sobrino et al., 2014; Helama et al., 2017), here we follow the chronology
420 proposed by Moreno et al. (2012): Dark Ages (DA, 1450-1050 cal yr BP); Medieval Climate Anomaly
421 (MCA, 1050-650 cal yr BP); and LIA (650-150 cal yr BP). Another climatic stage precedes the DA – the

422 Iberian Roman Humid Period (IRHP, 2600-1600 cal yr BP), originally described by Martín-Puertas et al.
423 (2008). However, in the LH record we have established different IRHP limits (2600-1450), based
424 accordingly to the pollen zonation (Fig. 3), and coinciding with the DA onset defined by Moreno et al.,
425 (2012).

426 The IRHP has been described as the wettest period in the western Mediterranean from proxies determined
427 both in marine and lacustrine records during the Late Holocene (Reed et al., 2001; Fletcher and Sanchez-
428 Goñi 2008; Combourieu-Nebout et al., 2009; Martín-Puertas et al., 2009; Nieto-Moreno et al., 2013;
429 Sánchez-López et al., 2016). A relative maximum in AP occurred in the LH record during this time, also
430 indicating forest development and relative high humidity during the Late Holocene in the area (zone LH-
431 4; Fig. 7). This is further supported by high K/Al and K/Ti ratios and MS values, indicating high detrital
432 input in the drainage basin, a minimum in Poaceae and low Saharan eolian input (low Ca/Al, Ca/Ti and
433 Zr/Al ratios) (Fig. 7). Fluvial elemental ratios have also shown an increase in river runoff in Alboran Sea
434 marine records (Nieto-Moreno et al., 2011; Rodrigo-Gámiz et al., 2011). This humid period seems to be
435 correlated with a solar maximum (Solanki et al., 2004) and persistent negative NAO conditions (Olsen et
436 al., 2012), which could have triggered general humid conditions in the Mediterranean. However, in the
437 LH record fluctuation in AP between 2300 and 1800 cal yr BP occurred, pointing to arid conditions at
438 that time. This arid event also seems to show up in BdIC, with a decrease in AP between 2400 and 1900
439 cal yr BP (Ramos-Román et al., 2016) and in Zoñar Lake, with water highly chemically concentrated and
440 gypsum deposition between 2140 and 1800 cal yr BP (Martín-Puertas et al., 2009). In Corchia Cave a
441 rapid excursion towards arid condition is recoded at ~2000 cal yr BP (Regattieri et al., 2014) (Fig.7). As
442 we explained in section 5, the apparently anomalous percentages of *Pinus* at this time, could be justified
443 by an upward migrations of the oromediterranean forest species triggered by higher temperatures and/or
444 the high pollen-production and dispersal of *Pinus*. Nevertheless, we cannot exclude others factors that
445 could influence the pollen transport such as the wind energy, mostly controlled by the NAO in the
446 southern Iberia. A persistent negative NAO phase, as occurred during the IRWP (Sánchez-López et al.,
447 2016), would have triggered more humid conditions and higher westerlies influence over southern
448 Europe. The higher occurrence of *Pinus* in the surrounding area due to the favourable climatic conditions,
449 along with the higher wind energy over Sierra Nevada and the characteristics of bisaccate pollen, could
450 have overstate the percentages of *Pinus* in our record.

451 **5.1.4. Dark Ages and Medieval Climate Anomaly (DA, MCA; 1450-650 cal yr BP)**

452 Predominantly arid conditions, depicted by high abundance of herbaceous and xerophytic species and an
453 AP minimum in the LH record, are shown for both DA and MCA (zone LH-5; Fig. 7). This is further
454 supported in this record by an increase in Saharan eolian input Ca/Al, Ca/Ti and Zr/Al ratios, and by a
455 decrease in surface runoff, indicated by the K/Al and K/Ti ratios (zone LH-5; Fig. 7). These results from
456 LH agree with climate estimations of overall aridity modulated by a persistent positive NAO phase during
457 this period (Trouet et al., 2009; Olsen et al., 2012), also previously noted by Ramos-Román et al. (2016)
458 in the area (Fig. 7).

459 Generally arid climate conditions during the DA and the MCA have also been previously described in the
460 LdIM and BdIC records, shown by a decrease in mesophytes and a rise of xerophytic vegetation during

461 that time (Jiménez-Moreno et al., 2013; Ramos-Román et al., 2016). Several pollen records in south and
462 central Iberian Peninsula also indicate aridity during the DA and MCA, for example grassland expanded
463 at Cañada de la Cruz, while in Siles Lake a lower occurrence of woodlands occurred (Carrión, 2002).
464 Also in Cimera Lake low lake level and higher occurrence of xerophytes were recorded (Sánchez-López
465 et al., 2016). Arid conditions were depicted in Zoñar Lake by an increase in *Pistacia* and heliophytes (i.e.,
466 Chenopodiaceae) and lower lake level (Martín-Puertas et al., 2010). Similar climatic conditions were
467 noticed in the marine records MD95-2043 and ODP 976 in the Alboran Sea through decreases in forest
468 (Fletcher and Sánchez-Goñi, 2008; Combourieu-Nebout et al., 2009; Fig. 7). Arid conditions in Basa de
469 la Mora (northern Iberian Peninsula) occurred during this time, characterized by maximum values of
470 *Artemisia*, and a lower development of deciduous *Quercus* and aquatic species such as *Potamogeton*, also
471 indicating low lake water levels (Moreno et al., 2012). Arid conditions were also documented by
472 geochemical data in marine records from the Alboran Sea (Nieto-Moreno et al., 2013, 2015), in the Gulf
473 of Lion and South of Sicily (Jalut et al., 2009). Aridity has also been interpreted for central Europe using
474 lake level reconstructions (Magny, 2004) and in speleothems records in central Italy (Regattieri et al.,
475 2014). Nevertheless, wetter conditions were recorded during the DA in some records from northern
476 Iberian Peninsula (Sánchez-López et al., 2016). Humid conditions depicted by higher lake level and less
477 salinity occurred in Arreo Lake (Corella et al., 2013). In Sanabria Lake, the dominance of planktonic
478 diatom *Aulacoseira subborealis* is interpreted as relative humid conditions at that time (Jambrina-
479 Enríquez et al., 2014). This heterogeneity in the climate during the DA is due to the existence of an N-S
480 humidity gradient in the Iberian Peninsula (Sánchez-López et al., 2016). Nonetheless, this gradient seems
481 to be more diffuse during the MCA, which is characterized as an overall arid period in the entire Iberian
482 Peninsula (Morellón et al., 2012; Sánchez-López et al., 2016).

483 **5.1.5. Little Ice Age (LIA; 650-150 cal yr BP)**

484 The LIA is interpreted as an overall humid period in the LH record. This is indicated by higher AP values
485 than during the MCA, low Saharan dust input (low Ca/Al, Ca/Ti and Zr/Al ratios), a decrease in herbs
486 (Poaceae) and high values in the K/Al and K/Ti ratios indicating enhanced runoff (zone LH-6A; Fig. 7).
487 An increase in fluvial-derived proxies has been previously documented in other Iberian terrestrial records
488 such as Basa de la Mora Lake (Moreno et al., 2012), Zoñar Lake (Martín-Puertas et al., 2010) or Cimera
489 Lake (Sánchez-López et al., 2016) and marine records from the Alboran Sea basin (Nieto-Moreno et al.,
490 2011, 2015). Lake level reconstructions in Estanya Lake, in the Pre-Pyrenees (NE Spain), have shown
491 high water levels during this period (Morellón et al., 2009, 2011), supporting our humid climate
492 inferences. Nevertheless, fluctuations in *Artemisia* during the LIA suggest an unstable period in Sierra
493 Nevada (Fig. 8), in agreement with the high variability in *Pinus*, *Artemisia*, and water availability
494 deduced from recent high-resolution studies in the neighbour BdIC and BdIV records (Ramos-Román et
495 al., 2016; García-Alix et al., 2017). The same pattern occurred in several Iberian records (Oliva et al.,
496 2018), revealing that the LIA was not a climatically stable period and many oscillations at short-time
497 scale occurred.

498 A persistently negative NAO phase, although with high variability, occurred during this period (Trouet et
499 al., 2009), which could explain the overall humid conditions observed in southern Europe. As in the Early

500 Holocene arid events, solar variability has been hypothesized as the main forcing of this climatic event
501 (Bond et al., 2001; Mayewski et al., 2004; Fletcher et al., 2013; Ramos-Román et al., 2016).

502 **5.1.6. Industrial Period (IP; 150 cal yr BP-Present)**

503 The IP is characterized by a sharp increase in the Pb/Al ratio in LH record (Fig. 8), suggesting more
504 mining, fossil fuel burning or other human industrial activities (García-Alix et al., 2013, 2017). This is
505 coeval with a rise in AP, which is also related to human activities such as *Olea* commercial cultivation at
506 lower elevations around Sierra Nevada or *Pinus* reforestation in the area (Fig. 7 and 8; Valbuena-
507 Carabaña et al., 2010; Anderson et al., 2011). The same pattern has also been observed in others records
508 from Sierra Nevada (Jiménez-Moreno and Anderson, 2012; García-Alix et al., 2013; Ramos-Román et
509 al., 2016), in Zoñar Lake and the Alboran Sea records (Martín-Puertas et al., 2010). In addition, a
510 progressively increasing trend in Zr/Al and Ca/Al ratios is observed during the last two centuries, which
511 could be related to increasing local aridity and/or anthropogenic desertification, but also with a change in
512 the origin and/or composition of the dust reaching to the lake (Jiménez-Espejo et al., 2014), likely related
513 to the beginning of extensive agriculture and the concomitant desertification in the Sahel region (Mulitza
514 et al., 2010).

515 **5.2. Significance of the eolian record from Laguna Hondera**

516 Saharan dust influence over current alpine lake ecosystems is widely known (Morales-Baquero et al.,
517 2006a, 2006b; Pulido-Villena et al., 2008b; Mladenov et al., 2011, Jiménez et al., 2018). The most
518 representative elements of Saharan dust in LH record are Fe, Zr and Ca as shown by the PC2 loading
519 (Fig. 5), where Ca and Fe directly affect the alpine lake biogeochemistry in this region (Pulido-Villena et
520 al., 2006, 2008b, Jiménez et al., 2018). Zirconium is transported in heavy minerals in eolian dust (Govin
521 et al., 2012) and has largely been used in the Iberian Peninsula and the western Mediterranean as an
522 indicator of eolian Saharan input (Moreno et al., 2006; Nieto-Moreno et al., 2011; Rodrigo-Gámiz et al.,
523 2011; Jiménez-Espejo et al., 2014; Martínez-Ruiz et al., 2015, and references therein). High Zr content
524 has also been identified in present aerosols at high elevations in Sierra Nevada (García-Alix et al., 2017).
525 Considering the low weatherable base cation reserves in LH bedrock catchment area, calcium is
526 suggested to be carried by atmospheric input of Saharan dust into alpine lakes in Sierra Nevada (Pulido-
527 Villena et al., 2006, see discussion; Morales-Baquero et al., 2013). This is the first time that the Ca signal
528 is properly recorded in a long record from Sierra Nevada. This could be explained by higher evaporation
529 rates at this site promoting annual lake desiccation that could prevent Ca water column dissolution and
530 using/recycling by organism, preserving better the original eolian signal. These elements have an essential
531 role as nutrients becoming winnowed and recycled rapidly in the oligotrophic alpine lake ecosystem
532 (Morales-Baquero et al., 2006b). This phenomenon has also been observed in other high-elevation lakes
533 where the phytoplankton is supported by a small and continually recycled nutrient pool (e.g., Sawatzky et
534 al., 2006).

535 The SEM observations further confirm the presence of Saharan dust in the lake sediments from LH and
536 the occurrence of Zircon, the main source of eolian Zr, which is relatively abundant (Fig. 6a). Quartz with
537 rounded morphologies (eolian erosion) are also frequent (Fig. 6b) in the uppermost part of the record as

538 well as REE rich minerals, such as monazite, which is typical from the Saharan-Sahel Corridor area
539 (Moreno et al., 2006) (Fig. 6c). In addition, the fact that the highest correlation between Ca and Zr
540 occurred after ~6300 cal yr BP, ($r=0.57$ $p<0.005$) along with the SEM observation and the low
541 availability of Ca in these ecosystems, could suggest that the beginning of Saharan dust arrivals to the
542 lake, including both elements, took place at this time, giving rise to the present way of nutrient inputs in
543 these alpine lakes (Morales-Baquero et al., 2006b; Pulido-Villena et al., 2006). The onset of Saharan dust
544 input into southern Iberia occurred prior to the end of the African Humid Period (AHP; ~5500 cal yr BP;
545 deMenocal et al., 2000), as previously noticed in the nearby LdRS (Jiménez-Espejo et al., 2014) and in
546 Alboran Sea (Rodrigo-Gámiz et al., 2011). This could suggest a progressive climatic deterioration in
547 North Africa, which culminated with the AHP demise and the massive Saharan dust input recorded in all
548 records in Sierra Nevada at ~3500 cal yr BP (Fig. 7).

549 **6. Conclusions**

550 The multiproxy paleoclimate analysis from LH has allowed the reconstruction of the vegetation and
551 climate evolution in Sierra Nevada and southern Iberia during the Holocene, and the possible factors that
552 have triggered paleoenvironmental changes. Climate during the Early Holocene was predominantly
553 humid, with two relatively arid periods between 10000 and 9000 and at ~8200 cal yr BP, resulting in less
554 detrital inputs and a change to more peaty lithology. The onset of an arid trend took place around 7000 cal
555 yr BP, decreasing the runoff input in the area. A significant increase in eolian-derived elements occurred
556 between 6300 and 5500 cal yr BP, coinciding with the AHP demise. An arid interval is recorded between
557 4000 and 2500 cal yr BP, with a vegetation assemblage dominated by xerophytes.

558 Relative humid conditions occurred in the area between 2500 and 1450 cal yr BP, interrupting the Late
559 Holocene aridification trend. This humid interval was characterized by expansion of forest vegetation,
560 high runoff input, and a more clayey lithology. However, during the DA and the MCA (1450-650 cal yr
561 BP) there was enhanced eolian input and an expansion of xerophytes, indicating increased arid
562 conditions. In contrast, the LIA (650-150 cal yr BP) was characterized by predominant humid conditions
563 as pointed out high runoff and low eolian input. The IP (150 cal yr BP-Present) is characterized in the LH
564 record by the highest values of the Pb/Al ratio, probably indicating fossil fuel burning by enhanced
565 mining and metallurgy industry. The increase in human activities at this time in this area can also be
566 deduced by the expansion of *Olea* cultivation at lower elevations and *Pinus* reforestation in the area.

567 Importantly, the LH record shows a unique and exceptional Ca signal derived from eolian input (high Ca-
568 Zr correlation) during the past ~6300 years in Sierra Nevada. The good preservation of the Ca record
569 might have been favoured by the high evaporation and the low lake depth, which could have prevented
570 Ca column water dissolution and its re-use by organisms. Our record indicate that present-day inorganic
571 nutrient input from Sahara was established 6300 yrs ago and lasted until the Present, with variations
572 depending on the prevailing climate.

573 **Acknowledgements**

574 This study was supported by the project P11-RNM 7332 of the “Junta de Andalucía”, the projects
575 CGL2013-47038-R, CGL2015-66830-R of the “Ministerio de Economía y Competitividad of Spain and

576 Fondo Europeo de Desarrollo Regional FEDER”, the research groups RNM0190 and RNM179 (Junta de
577 Andalucía). We also thank to Unidad de Excelencia (UCE-PP2016-05). J.M.M.F acknowledges the PhD
578 funding provided by Ministerio de Economía y Competitividad (CGL2015-66830-R) A.G.-A. was also
579 supported by a Marie Curie Intra-European Fellowship of the 7th Framework Programme for Research,
580 Technological Development and Demonstration of the European Commission (NAOSIPUK. Grant
581 Number: PIEF-GA-2012-623027) and by a Ramón y Cajal Fellowship RYC-2015-18966 of the Spanish
582 Government (Ministerio de Economía y Competitividad) and M.R.G. from the Andalucía Talent Hub
583 Program co-funded by the European Union’s Seventh Framework Program (COFUND – Grant
584 Agreement nº 291780) and the Junta de Andalucía. We thank Santiago Fernández, Maria Dolores
585 Hernandez and Antonio Mudarra for their help recovering the core and Inés Morales for the initial core
586 description and MS data. We thank Jaime Frigola (Universitat de Barcelona) for his help with XRF core
587 scanning. We would also like to thank Nathalie Combourieu Nebout, and the two anonymous reviewers
588 for their comments and suggestions, which improved the paper.

589 **References**

- 590 Anderson, R. S., Jiménez-Moreno, G., Carrión, J. S., and Pérez-Martínez, C.: Holocene vegetation history
591 from Laguna de Río Seco, Sierra Nevada, southern Spain, *Quaternary Sci. Rev.* 30, 1615-1629,
592 DOI:10.1016/j.quascirev.2011.03.005, 2011.
- 593 Andrade, A., Valdeolillos, A., and Ruíz-Zapata, B.: Modern pollen spectra and contemporary
594 vegetation in the Paramera Mountain range (Ávila, Spain), *Rev. Palaeobot. Palyno.*, 82, 127-139,
595 DOI:10.1016/0034-6667(94)90024-8, 1994.
- 596 Ariztegui, D., Asioli, A., Lowe, J. J., Trincardi, F., Vigliotti, L., Tamburini, F., Chondrogianni, C.,
597 Accorsi, C. A., Bandini Mazzanti, M., Mercuri, A. M., Van der Kaars, S., McKenzie, J. A., and Oldfield,
598 F.: Palaeoclimate and the formation of sapropel S1: inferences from Late Quaternary lacustrine and
599 marine sequences in the central Mediterranean region, *Palaeogeogr. Palaeocl.*, 158, 215-240,
600 DOI:10.1016/S0031-0182(00)00051-1, 2000.
- 601 Aubet, M. E.: *The Phoenicians and the West: Politics, colonies and trade*, Cambridge University Press,
602 Cambridge, 2001.
- 603 Ávila, A., Queralt-Mitjans, I., and Alarcón, M.: Mineralogical composition of African dust delivered by
604 red rains over northeastern Spain, *J. Geophys. Res.-Atmos.*, 102, 21977-21996, DOI:10.1029/97JD00485,
605 1997.
- 606 Ballantyne, A. P., Brahney, J., Fernandez, D., Lawrence, C. L., Saros, J., and Neff, J. C.: Biogeochemical
607 response of alpine lakes to a recent increase in dust deposition in the Southwestern US, *Biogeosciences*,
608 8, 2689, DOI:10.5194/bg-8-2689-2011, 2011.
- 609 Bar-Matthews, M., Ayalon, A., and Kaufman, A.: Timing and hydrological conditions of sapropel events
610 in the Eastern Mediterranean, as evident from speleothems, Soreq cave, Israel, *Chem. Geol.*, 169, 145-
611 156, DOI:10.1016/S0009-2541(99)00232-6, 2000.

612 Bahr, A., Jiménez-Espejo, F. J., Kolasinac, N., Grunert, P., Hernández-Molina, F. J., Röhl, U., Voelker,
613 A. H. L., Escutia, C., Stow, D. A. V., Hodell, D., and Alvarez-Zarikian, C. A.: Deciphering bottom
614 current velocity and paleoclimate signals from contourite deposits in the Gulf of Cádiz during the last 140
615 kyr: An inorganic geochemical approach, *Geochem. Geophys. Geosy.*, 15, 3145-3160,
616 DOI:10.1002/2014GC005356, 2014.

617 Blaauw, M.: Methods and code for 'classical' age-modelling of radiocarbon sequences, *Quat.*
618 *Geochronol.*, 5, 512-518, DOI:10.1016/j.quageo.2010.01.002, 2010.

619 Bea, F.: Residence of REE, Y, Th and U in granites and crustal protoliths: implications for the chemistry
620 of crustal melts, *J. Petrol.*, 37, 521-532, DOI:10.1093/petrology/37.3.521, 1996.

621 Beug, H. J.: *Leitfaden der Pollenbestimmung für Mitteleuropa und angrenzende Gebiete*, Fischer,
622 Stuttgart, 2004.

623 Bond, G., Showers, W., Cheseby, M., Lotti, R., Almasi, P., deMenocal, P., Priore, P., Cullen, H., Hajdas,
624 I., and Bonani, G.: A pervasive millennial-scale cycle in North Atlantic Holocene and glacial climates,
625 *Science*, 278, 1257-1266, DOI:10.1126/science.278.5341.1257, 1997.

626 Bond, G., Kromer, B., Beer, J., Muscheler, R., Evans, M., Showers, W., Hoffmann, S., Lotti-Bond, R.,
627 Hajdas, I., and Bonani, G.: Persistent solar influence on North Atlantic climate during the Holocene,
628 *Science*, 294, 2130-2136, DOI:10.1126/science.1065680, 2001.

629 Cacho, I., Grimalt, J. O., and Canals, M.: Response of the Western Mediterranean Sea to rapid climatic
630 variability during the last 50,000 years: a molecular biomarker approach, *J. Marine Syst.*, 33-34, 253-272,
631 DOI:10.1016/S0924-7963(02)00061-1, 2002.

632 Calvert, S. E., and Pedersen, T. F.: *Elemental proxies for palaeoclimatic and palaeoceanographic*
633 *variability in marine sediments: interpretation and application*, *Proxies in Late Cenozoic*
634 *Paleoceanography*, Elsevier, Amsterdam, 2007.

635 Carrión, J. S.: Patterns and processes of Late Quaternary environmental change in a montane region of
636 southwestern Europe, *Quaternary Sci. Rev.*, 21, 2047-2066, DOI:10.1016/S0277-3791(02)00010-0, 2002.

637 Carrión, J. S., Munuera, M., Dupré, M., and Andrade, A.: Abrupt vegetation changes in the Segura
638 mountains of southern Spain throughout the Holocene, *J. Ecol.*, 89, 783-797, DOI:10.1046/j.0022-
639 0477.2001.00601.x, 2001.

640 Carrión, J. S., Sánchez-Gómez, P., Mota, J. F., Yll, E. I., and Chaín, C.: Fire and grazing are contingent on
641 the Holocene vegetation dynamics of Sierra de Gádor, southern Spain, *Holocene* 13, 839-849,
642 DOI:10.1191/0959683603hl662rp, 2003.

643 Carrión, J. S., Fuentes, N., González-Sampériz, P., Sánchez Quirante, L., Finlayson, J. C., Fernández, S.,
644 and Andrade, A.: Holocene environmental change in a montane region of southern Europe with a long
645 history of human settlement, *Quaternary Sci. Rev.*, 26, 1455-1475, DOI:10.1016/j.quascirev.2007.03.013,
646 2007.

- 647 Carrión, J. S., Fernández, S., González-Sampérez, P., Gil-Romera, G., Badal, E., Carrión-Marco, Y.,
648 López-Merino, L., López-Sáez, J. A., Fierro, E., and Burjachs, F.: Expected trends and surprises in the
649 Lateglacial and Holocene vegetation history of the Iberian Peninsula and Balearic Islands, *Rev.*
650 *Palaeobot. Palyno.*, 162, 458-476, DOI:10.1016/j.jaridenv.2008.11.014, 2010.
- 651 Castillo Martín, A.: *Lagunas de Sierra Nevada*, Universidad de Granada, Granada, 2009.
- 652 Combourieu Nebout, N., Turon, J. L., Zahn, R., Capotondi, L., Londeix, L., and Pahnke, K.: Enhanced
653 aridity and atmospheric high-pressure stability over the western Mediterranean during the North Atlantic
654 cold events of the past 50 ky, *Geology*, 30, 863-866, DOI:10.1130/0091-
655 7613(2002)030<0863:EAAAHP>2.0.CO;2, 2002.
- 656 Combourieu Nebout, N., Peyron, O., Dormoy, I., Desprat, S., Beaudouin, C., Kotthoff, U., and Marret, F.:
657 Rapid climatic variability in the west Mediterranean during the last 25,000 years from high resolution
658 pollen data, *Clim. Past*, 5, 503-521, DOI:10.5194/cpd-5-671-2009, 2009.
- 659 Comero, S., Locoro, G., Free, G., Vaccaro, S., De Capitani, L., and Gawlik, B. M.: Characterisation of
660 Alpine lake sediments using multivariate statistical techniques, *Chemometr. Intell. Lab.*, 107(1), 24-30,
661 DOI:10.1016/j.chemolab.2011.01.002, 2011.
- 662 Corella, J. P., Stefanova, V., El Anjoumi, A., Rico, E., Giralt, S., Moreno, A., Plata-Monter, A., and
663 Valero-Garcés, B. L.: A 2500-year multi-proxy reconstruction of climate change and human activities in
664 northern Spain: the Lake Arreo record, *Palaeogeogr. Palaeoclimatol. Palaeoecol.*, 386, 555-568,
665 DOI:10.1016/j.palaeo.2013.06.022, 2013.
- 666 Davis, J. C., and Sampson, R. J.: *Statistics and data analysis in geology*, Wiley, New York, 1986.
- 667 de Lange, G. J., Thomson, J., Reitz, A., Slomp, C. P., Principato, M. S., Erba, E., and Corselli, C.:
668 Synchronous basin-wide formation and redox-controlled preservation of a Mediterranean sapropel, *Nat.*
669 *Geosci.*, 1, 606-610, DOI:10.1038/ngeo283, 2008.
- 670 deMenocal, P., Ortiz, J., Guilderson, T., Adkins, J., Sarnthein, M., Baker, L., and Yarusinsky, M.: Abrupt
671 onset and termination of the African Humid Period: rapid climate responses to gradual insolation forcing,
672 *Quaternary Sci. Rev.*, 19, 347-361, DOI:10.1016/S0277-3791(99)00081-5, 2000.
- 673 Díaz de Federico, A.: *Estudio geológico del Complejo de Sierra Nevada en la transversal del Puerto de la*
674 *Ragua (Cordillera Bética)*, Ph.D. thesis, Universidad de Granada, Granada, 1980.
- 675 El Aallali, A., López Nieto, J. M., Pérez Raya, F., and Molero Mesa, J.: Estudio de la vegetación forestal
676 en la vertiente sur de Sierra Nevada (Alpujarra Alta granadina), *Itinera Geobot.*, 11, 387-402, 1998.
- 677 Faegri, K., and Iversen, J.: *Textbook of Pollen Analysis*, Wiley, New York, 1989.
- 678 Fletcher, W. J., Boski, T., and Moura, D.: Palynological evidence for environmental and climatic change
679 in the lower Guadiana valley, Portugal, during the last 13 000 years, *Holocene*, 17, 481-494,
680 DOI:10.1177/0959683607077027, 2007.

681 Fletcher, W. J., and Sánchez Goñi, M. F.: Orbital- and sub-orbital-scale climate impacts on vegetation of
682 the western Mediterranean basin over the last 48,000 yr, *Quaternary Res.*, 70, 451-464,
683 DOI:10.1016/j.yqres.2008.07.002, 2008.

684 Fletcher, W. J., Sánchez Goñi, M. F., Peyron, O., and Dormoy, I.: Abrupt climate changes of the last
685 deglaciation detected in a Western Mediterranean forest record, *Clim. Past*, 6, 245-264, DOI:10.5194/cp-
686 6-245-2010, 2010.

687 Fletcher, W. J., and Zielhofer, C.: Fragility of Western Mediterranean landscapes during Holocene rapid
688 climate changes, *Catena*, 103, 16-29, DOI:10.1016/j.catena.2011.05.001, 2013.

689 García-Alix, A., Jiménez-Moreno, G., Anderson, R. S., Jiménez-Espejo, F. J., and Delgado-Huertas, A.:
690 Holocene paleoenvironmental evolution of a high-elevation wetland in Sierra Nevada, southern Spain,
691 deduced from an isotopic record, *J. Paleolimnol.*, 48, 471-484, DOI:10.1007/s10933-012-9625-2, 2012.

692 García-Alix, A., Jiménez-Espejo, F. J., Lozano, J. A., Jiménez-Moreno, G., Martínez-Ruiz, F., García
693 Sanjuán, L., Aranda Jiménez, G., García Alfonso, E., Ruiz-Puertas, G., and Anderson, R. S.:
694 Anthropogenic impact and lead pollution throughout the Holocene in Southern Iberia, *Sci. Total Environ.*,
695 449, 451-460, DOI:10.1016/j.scitotenv.2013.01.081, 2013.

696 García-Alix, A., Jimenez Espejo, F. J., Toney, J. L., Jiménez-Moreno, G., Ramos-Román, M. J.,
697 Anderson, R. S., Ruano, P., Queralt, I., Delgado Huertas, A., and Kuroda, J.: Alpine bogs of southern
698 Spain show human-induced environmental change superimposed on long-term natural variations, *Sci.*
699 *Rep.-UK*, 7, 7439, DOI:10.1038/s41598-017-07854-w, 2017.

700 García-Alix, A., Jiménez-Espejo, F.J., Jiménez-Moreno, G., Toney, J.L., Ramos-Román, M.J., Camuera,
701 J., Anderson, R.S., Delgado-Huertas, A., Martínez-Ruiz, F., and Queralt, I.: Holocene geochemical
702 footprint from Semi-arid alpine wetlands in southern Spain, *Sci. Data*, 5, 180024,
703 DOI:10.1038/sdata.2018.24, 2018.

704 Govin, A., Holzwarth, U., Heslop, D., Ford Keeling, L., Zabel, M., Mulitza, S., Collins, J. A., and
705 Chiessi, C. M.: Distribution of major elements in Atlantic surface sediments (36°N-49°S): imprint of
706 terrigenous input and continental weathering, *Geochem. Geophys. Geosy.*, 13, Q01013,
707 DOI:10.1029/2011GC003785, 2012.

708 Grimm, E. C.: CONISS: a Fortran 77 program for stratigraphically constrained cluster analysis by the
709 method of incremental sum of squares, *Comput. Geosci.*, 13, 13-35, DOI:10.1016/0098-3004(87)90022-
710 7, 1987.

711 Grimm, E.: *TILIA: a pollen program for analysis and display*, Illinois State Museum, Springfield, 1993.

712 Hammer, Ø., Harper, D. A. T., and Ryan, P. D.: *Paleontological Statistics Software Package for*
713 *Education and Data Analysis*, *Palaeontol. electron.*, 4, 1-9, 2001.

714 Harper, D. A. T.: *Numerical Palaeobiology*, John Wiley & Sons, Chichester, 1999.

715 Helama, S., Jones, P. D., and Briffa, K. R.: Dark Ages Cold Period: A literature review and directions for
716 future research, *Holocene* 27, 1600-1606, DOI: 10.1177/0959683617693898, 2017.

717 Jalut, G., Esteban Amat, A., Bonnet, L., Gauquelin, T., and Fontugne, M.: Holocene climatic changes in
718 the Western Mediterranean, from south-east France to south-east Spain, *Palaeogeogr. Palaeocli.*, 160, 255-
719 290, DOI:10.1016/S0031-0182(00)00075-4, 2000.

720 Jalut, G., Dedoubat, J. J., Fontugne, M., and Otto, T.: Holocene circum-Mediterranean vegetation
721 changes: climate forcing and human impact, *Quatern. Int.*, 200, 4-18, DOI:10.1016/j.quaint.2008.03.012,
722 2009.

723 Jambrina-Enrriquez, M., Rico, M., Moreno, A., Leira, M., Bernárdez, P., Prego, R., Recio, C., and Valero-
724 Garcés, B. L.: Timing of deglaciation and postglacial environmental dynamics in NW Iberia: the Sanabria
725 Lake record, *Quaternary Sci. Rev.*, 94, 136-158, DOI:10.1016/j.quascirev.2014.04.018, 2014.

726 Jiménez, L., Rühland, K. M., Jeziorski, A., Smol, J. P., and Pérez-Martínez, C.: Climate change and
727 Saharan dust drive recent cladoceran and primary production changes in remote alpine lakes of Sierra
728 Nevada, Spain, *Glob. Change Biol.*, 24, e139-e158, DOI:10.1111/gcb.13878, 2018.

729 Jiménez-Espejo, F. J., Martínez-Ruiz, F., Rogerson, M., González-Donoso, J. M., Romero, O., Linares,
730 D., Sakamoto, T., Gallego-Torres, D., Rueda Ruiz, J. L., Ortega-Huertas, M., and Perez Claros, J. A.:
731 Detrital input, productivity fluctuations, and water mass circulation in the westernmost Mediterranean Sea
732 since the Last Glacial Maximum, *Geochem. Geophys. Geosy.*, 9, Q11U02, DOI:10.1029/2008GC002096,
733 2008.

734 Jiménez-Espejo, F. J., García-Alix, A., Jiménez-Moreno, G., Rodrigo-Gámiz, M., Anderson, R. S.,
735 Rodríguez-Tovar, F. J., Martínez-Ruiz, F., Giralt, S., Delgado-Huertas, A., and Pardo-Igúzquiza, E.:
736 Saharan aeolian input and effective humidity variations over western Europe during the Holocene from a
737 high altitude record, *Chem. Geol.*, 374, 1-12, DOI:10.1016/j.chemgeo.2014.03.001, 2014.

738 Jiménez-Moreno, G., and Anderson, R. S.: Holocene vegetation and climate change recorded in alpine
739 bog sediments from the Borreguiles de la Virgen, Sierra Nevada, southern Spain, *Quaternary Res.*, 77, 44-
740 53, DOI:10.1016/j.yqres.2011.09.006, 2012.

741 Jiménez-Moreno, G., García-Alix, A., Hernández-Corbalán, M. D., Anderson, R. S., and Delgado-
742 Huertas, A.: Vegetation, fire, climate and human disturbance history in the southwestern Mediterranean
743 area during the late Holocene, *Quaternary Res.*, 79, 110-122, DOI:10.1016/j.yqres.2012.11.008, 2013.

744 Jiménez-Moreno, G., Rodríguez-Ramírez, A., Pérez-Asensio, J. N., Carrión, J. S., López-Sáez, J. A.,
745 Villarías-Robles, J. J. R., Celestino-Pérez, S., Cerrillo-Cuenca, E., Ángel León, A., and Contreras, C.:
746 Impact of late-Holocene aridification trend, climate variability and geodynamic control on the
747 environment from a coastal area in SW Spain, *Holocene*, 25, 607-617, DOI:10.1177/0959683614565955,
748 2015.

749 Lionello, P., Malanotte-Rizzoli, P., Boscolo, R., Alpert, P., Artale, V., Li, L., Luterbacher, J., May, W.,
750 Trigo, R., Tsimplis, M., Ulbrich, U., and Xoplaki, E.: The Mediterranean climate: an overview of the
751 main characteristics and issues, *Developments in Earth and Environmental Sciences*, 4, Elsevier,
752 Amsterdam, Netherlands, 1-26, 2006.

753 Liu, Z., Wang, Y., Gallimore, R., Gasse, F., Johnson, T., deMenocal, P., Adkins, J., Notaro, M., Prentice,
754 I. C., Kutzbach, J., Jacob, R., Behling, P., Wang, L., and Ong, E.: Simulating the transient evolution and
755 abrupt change of Northern Africa atmosphere–ocean–terrestrial ecosystem in the Holocene. *Quaternary*
756 *Sci. Rev.*, 26, 1818-1837, DOI:10.1016/j.quascirev.2007.03.002, 2007.

757 Löwemark, L., Chen, H.-F., Yang, T.-N., Kylander, M., Yu, E.-F., Hsu, Y.-W., Lee, T.-Q., Song, S.-R.,
758 and Jarvis, S.: Normalizing XRF-scanner data: a cautionary note on the interpretation of high-resolution
759 records from organic-rich lakes, *J. Asian Earth Sci.*, 40, 1250-1256, DOI:10.1016/j.jseaes.2010.06.002,
760 2011.

761 Magny, M., Miramont, C., and Sivan, O.: Assessment of the impact of climate and anthropogenic factors
762 on Holocene Mediterranean vegetation in Europe on the basis of palaeohydrological records,
763 *Palaeogeogr. Palaeoclimatol.*, 186, 47-59, DOI:10.1016/S0031-0182(02)00442-X, 2002.

764 Magny, M., and Bégeot, C.: Hydrological changes in the European midlatitudes associated with
765 freshwater outbursts from Lake Agassiz during the Younger Dryas event and the early Holocene,
766 *Quaternary Res.*, 61, 181-192, doi:10.1016/j.yqres.2003.12.003, 2004.

767 Magny, M., de Beaulieu, J.-L., Drescher-Schneider, R., Vanni re, B., Walter-Simonnet, A.-V., Miras, Y.,
768 Millet, L., Bossuet, G., Peyron, O., Brugiapaglia, E., and Leroux, A.: Holocene climate changes in the
769 central Mediterranean as recorded by lake-level fluctuations at Lake Accesa (Tuscany, Italy), *Quaternary*
770 *Sci. Rev.*, 26, 1736-1758, DOI:10.1016/j.quascirev.2007.04.014, 2007.

771 Magny, M., Peyron, O., Sadori, L., Ortu, E., Zanchetta, G., Vanni re, B., and Tinner, W.: Contrasting
772 patterns of precipitation seasonality during the Holocene in the south- and north-central Mediterranean, *J.*
773 *Quat. Sci.*, 27, 290-296, DOI:10.1002/jqs.1543, 2012.

774 Mart n-Puertas, C., Valero-Garc s, B. L., Mata, M. P., Gonz lez-Samp riz, P., Bao, R., Moreno, A., and
775 Stefanova, V.: Arid and humid phases in southern Spain during the last 4000 years: the Zonar Lake
776 record, Cordoba, Holocene, 18, 907-921, DOI:10.1177/0959683608093533, 2008.

777 Mart n-Puertas, C., Valero-Garc s, B. L., Brauer, A., Mata, M. P., Delgado-Huertas, A., and Dulski, P.:
778 The Iberian–Roman Humid Period (2600–1600 cal yr BP) in the Zo nar Lake varve record (Andaluc a,
779 southern Spain), *Quaternary Res.*, 71, 108-120, DOI:10.1016/j.yqres.2008.10.004, 2009.

780 Mart n-Puertas, C., Jim nez-Espejo, F., Mart nez-Ruiz, F., Nieto-Moreno, V., Rodrigo, M., Mata, M. P.,
781 and Valero-Garc s, B. L.: Late Holocene climate variability in the southwestern Mediterranean region: an
782 integrated marine and terrestrial geochemical approach, *Clim. Past*, 6, 807-816, DOI:10.5194/cp-6-807-
783 2010, 2010.

784 Mart nez-Ruiz, F., Kastner, M., Gallego-Torres, D., Rodrigo-G miz, M., Nieto-Moreno, V., and Ortega-
785 Huertas, M.: Paleoclimate and paleoceanography over the past 20,000 yr in the Mediterranean Sea Basins
786 as indicated by sediment elemental proxies, *Quaternary Sci. Rev.*, 107, 25-46,
787 DOI:10.1016/j.quascirev.2014.09.018, 2015.

788 Mayewski, P. A., Rohling, E. E., Curt Stager, J., Karl n, W., Maasch, K. A., David Meeker, L.,
789 Meyerson, E. A., Gasse, F., van Kreveld, S., Holmgren, K., Lee-Thorp, J., Rosqvist, G., Rack, F.,

790 Staubwasser, M., Schneider, R. R., and Steig, E. J.: Holocene climate variability, *Quaternary Res.* 62,
791 243-255, DOI:10.1016/j.yqres.2004.07.001, 2004.

792 Mladenov, N., Pulido-Villena, E., Morales-Baquero, R., Ortega-Retuerta, E., Sommaruga, R., and Reche,
793 I.: Spatiotemporal drivers of dissolved organic matter in high alpine lakes: Role of Saharan dust inputs
794 and bacterial activity, *J. Geophys. Res.-Biogeo.*, 113, DOI:10.1029/2008JG000699, 2008.

795 Mladenov, N., Sommaruga, R., Morales-Baquero, R., Laurion, I., Camarero, L., Diéguez, M. C.,
796 Camacho, A., Delgado, A., Torres, O., Chen, Z., Felip, M., and Reche, I.: Dust inputs and bacteria
797 influence dissolved organic matter in clear alpine lakes, *Nat. Commun.* 2, 405,
798 DOI:10.1038/ncomms1411, 2011.

799 Morales-Baquero, R., Carrillo, P., Reche, I., and Sánchez-Castillo, P.: Nitrogen-phosphorus relationship
800 in high mountain lakes: effects of the size of catchment basins, *Can. J. Fish. Aquat. Sci.*, 56, 1809-1817,
801 DOI:10.1139/cjfas-56-10-1809, 1999.

802 Morales-Baquero, R., Pulido-Villena, E., and Reche, I.: Atmospheric inputs of phosphorus and nitrogen
803 to the southwest Mediterranean region: Biogeochemical responses of high mountain lakes, *Limnol.*
804 *Oceanogr.*, 51, 830-837, DOI:10.4319/lo.2006.51.2.0830, 2006a.

805 Morales-Baquero R., Pulido-Villena, E., Romera, O., Ortega-Retuerta, E., Conde-Porcuna, J. M., Pérez-
806 Martínez, C., and Reche, I.: Significance of atmospheric deposition to freshwater ecosystems in the
807 southern Iberian Peninsula, *Limnetica*, 25, 171-180, 2006b.

808 Morales-Baquero, R., Pulido-Villena, E., and Reche, I.: Chemical signature of Saharan dust on dry and
809 wet atmospheric deposition in the south-western Mediterranean region, *Tellus B*, 65,
810 DOI:10.3402/tellusb.v65i0.18720, 2013.

811 Morales-Baquero, R., and Pérez-Martínez C.: Saharan versus local influence on atmospheric aerosol
812 deposition in the southern Iberian Peninsula: Significance for N and P inputs, *Global Biogeochem.*
813 *Cycles*, 30, 501-513, DOI:10.1002/2015GB005254, 2016.

814 Moreno, A., Pérez, A., Frigola, J., Nieto-Moreno, V., Rodrigo-Gámiz, M., Martrat, B., González-
815 Sampéris, P., Morellón, M., Martín-Puertas, C., Corella, J. P., Belmonte, A., Sancho, C., Cacho, I.,
816 Herrera, G., Canals, M., Grimalt, J. O., Jiménez-Espejo, F. J., Martínez-Ruiz, F., Vegas-Villarrúbia, T.,
817 and Valero-Garcés, B. L.: The Medieval Climate Anomaly in the Iberian Peninsula reconstructed from
818 marine and lake records, *Quaternary Sci. Rev.*, 42, 16-32, DOI:10.1016/j.quascirev.2012.04.007, 2012.

819 Moreno, T., Querol, X., Castillo, S., Alastuey, A., Cuevas, E., Herrmann, L., Mounkaila, M., Elvira, J.,
820 Gibbons, W.: Geochemical variations in aeolian mineral particles from the Sahara–Sahel Dust Corridor.
821 *Chemosphere*, 65, 261-270, DOI:10.1016/j.chemosphere.2006.02.052, 2006.

822 Morellón, M., Valero-Garcés, B., Vegas-Vilarrúbia, T., González-Sampéris, P., Romero, O., Delgado-
823 Huertas, A., Mata, P., Moreno, A., Rico, M., and Corella, J. P.: Lateglacial and Holocene
824 palaeohydrology in the western Mediterranean region: the Lake Estanya record (NE Spain), *Quaternary*
825 *Sci. Rev.*, 28, 2582-2599, DOI:10.1016/j.quascirev.2009.05.014, 2009.

- 826 Morellón, M., Valero-Garcés, B., González-Sampériz, P., Vegas-Vilarrúbia, T., Rubio, E., Rieradevall,
827 M., Delgado-Huertas, A., Mata, P., Romero, O., Engstrom, D. R., López-Vicente, M., Navas, A., and
828 Soto, J.: Climate changes and human activities recorded in the sediments of Lake Estanya (NE Spain)
829 during the Medieval Warm Period and Little Ice Age, *J. Paleolimnol.*, 46, 423-452, DOI:10.1007/s10933-
830 009-9346-3, 2011.
- 831 Morellón, M., Pérez-Sanz, A., Corella, J. P., Büntgen, U., Catalán, J., González-Samprizé, P., González-
832 Trueba, J. J., López-Sáez, J. A., Moreno, A., Pla, S., Saz-Sánchez, M. Á., Scussolini, P., Serrano, E.,
833 Steinhilber, F., Stefanova, V., Vegas-Vilarrúbia, T., and Saz-Sánchez, M. A.: A multi-proxy perspective
834 on millennium-long climate variability in the Southern Pyrenees, *Clim. Past*, DOI:10.5194/cpd-7-3049-
835 2011, 2012.
- 836 Mulitza, S., Heslop, D., Pittauerova, D., Fischer, H. W., Meyer, I., Stuut, J.-B., Zabel, M., Mollenhauer,
837 G., Collins, J.A., Kuhnert, H., and Schulz, M.: Increase in African dust flux at the onset of commercial
838 agriculture in the Sahel region, *Nature*, 466, 226-228, DOI:10.1038/nature09213, 2010.
- 839 Sobrino, C. M., García-Moreiras, I., Castro, Y., Carreño, N. M., de Blas, E., Rodríguez, C. F., Judd, A.,
840 and García-Gil, S., Climate and anthropogenic factors influencing an estuarine ecosystem from NW
841 Iberia: new high resolution multiproxy analyses from San Simón Bay (Ría de Vigo), *Quaternary Sci.*
842 *Rev.*, 93, 11-33, DOI:10.1016/j.quascirev.2014.03.021, 2014.
- 843 Nieto-Moreno, V., Martínez-Ruiz, F., Giralt, S., Jiménez-Espejo, F. J., Gallego-Torres, D., Rodrigo-
844 Gámiz, M., García-Orellana, J., Ortega-Huertas, M., and de Lange, G. J.: Tracking climate variability in
845 the western Mediterranean during the Late Holocene: a multiproxy approach, *Clim. Past*, 7, 1395-1414,
846 DOI:10.5194/cp-7-1395-2011, 2011.
- 847 Nieto-Moreno, V., Martínez-Ruiz, F., Willmott, V., García-Orellana, J., Masqué, P., and Damsté, J. S.:
848 Climate conditions in the westernmost Mediterranean over the last two millennia: An integrated
849 biomarker approach, *Org. Geochem.*, 55, 1-10. DOI:10.1177/0959683613484613, 2013
- 850 Nieto-Moreno, V., Martínez-Ruiz, F., Gallego-Torres, D., Giralt, S., García-Orellana, J., Masqué, P.,
851 Sinninghe Damsté, J. S., and Ortega-Huertas, M.: Palaeoclimate and palaeoceanographic conditions in the
852 westernmost Mediterranean over the last millennium: an integrated organic and inorganic approach, *J.*
853 *Geol. Soc. London*, 172, 264-271, DOI:10.1144/jgs2013-105, 2015.
- 854 Oliva, M., Ruiz-Fernández, J., Barriendos, M., Benito, G., Cuadrat, J. M., Domínguez-Castro, F., García-
855 Ruiz, J. M., Giralt, S., Gómez-Ortiz, A., Hernández, A., López-Costas, O., López-Moreno, J. I., López-
856 Sáez, J. A., Matínez-Cortízar, A., Moreno, A., Prohom, M., Saz, M. A. Serrano, E., Tejedor, E., Trigo, R.,
857 Valero-Garcés, B. and López-Costas, O.: The Little Ice Age in Iberian mountains, *Earth-Sci. Rev.*, 177,
858 175-208, DOI:10.1016/j.earscirev.2017.11.010, 2018.
- 859 Olsen, J., Anderson, N. J., and Knudsen, M. F.: Variability of the North Atlantic Oscillation over the past
860 5,200 years, *Nat. Geosci.*, 5, 808-812, DOI:10.1038/ngeo1589, 2012.

- 861 Palma, P., Oliva, M., García-Hernández, C., Ortiz, A. G., Ruiz-Fernández, J., Salvador-Franch, F., and
862 Catarineu, M.: Spatial characterization of glacial and periglacial landforms in the highlands of Sierra
863 Nevada (Spain), *Sci. Total Environ.*, 584, 1256-1267, DOI:10.1016/j.scitotenv.2017.01.196, 2017.
- 864 Poska, A., and Pidek, I. A.: Pollen dispersal and deposition characteristics of *Abies alba*, *Fagus sylvatica*
865 and *Pinus sylvestris*, Roztocze region (SE Poland). *Veg. Hist. Archaeobot.*, 19, 91-101,
866 DOI:10.1007/s00334-009-0230-x, 2010.
- 867 Pulido-Villena, E., Reche, I., and Morales-Baquero, R.: Significance of atmospheric inputs of calcium
868 over the southwestern Mediterranean region: High mountain lakes as tools for detection, *Global*
869 *Biogeochem. Cy.*, 20, GB2012, DOI:10.1029/2005GB002662, 2006.
- 870 Pulido-Villena, E., Wagener, T., and Guieu, C.: Bacterial response to dust pulses in the western
871 Mediterranean: Implications for carbon cycling in the oligotrophic ocean, *Global Biogeochem. Cy.*, 22,
872 DOI:10.1029/2007GB003091, 2008a.
- 873 Pulido-Villena, E., Reche, I., and Morales-Baquero, R.: Evidence of an atmospheric forcing on
874 bacterioplankton and phytoplankton dynamics in a high mountain lake, *Aquat. sci.*, 70, 1-9,
875 DOI:10.1007/s00027-007-0944-8, 2008b.
- 876 Ramos-Román, M. J., Jiménez-Moreno, G., Anderson, R. S., García-Alix, A., Toney, J. L., Jiménez-
877 Espejo, F. J., and Carrión, J. S.: Centennial-scale vegetation and North Atlantic Oscillation changes
878 during the Late Holocene in the southern Iberia, *Quaternary Sci. Rev.*, 143, 84-95,
879 DOI:10.1016/j.quascirev.2016.05.007, 2016.
- 880 Ramos-Román, M. J.: Holocene paleoenvironmental change, climate and human impact in Sierra Nevada,
881 Southern Iberian Peninsula, Ph. D. Thesis, Universidad de Granada, Granada, 2018.
- 882 Ramos-Román, M. J., Jiménez-Moreno, G., Camuera, J., García-Alix, A., Anderson, R. S., Jiménez-
883 Espejo, F. J., Sasche, D., Toney, J. L., Carrión, J. S., Webster, C and Yanes, Y.: Millennial-scale cyclical
884 environment and climate variability during the Holocene in the western Mediterranean region deduced
885 from a new multi-proxy analysis from the Padul record (Sierra Nevada, Spain), *Glob. Planet. Change*,
886 168, 35-53, DOI:10.1016/j.gloplacha.2018.06.003, 2018a.
- 887 Ramos-Román, M. J., Jiménez-Moreno, G., Camuera, J., García-Alix, A., Anderson, R. S., Jiménez-
888 Espejo, F. J., and Carrión, J. S.: Holocene climate aridification trend and human impact interrupted by
889 millennial-and centennial-scale climate fluctuations from a new sedimentary record from Padul (Sierra
890 Nevada, southern Iberian Peninsula), *Clim. Past*, 14, 117-137, DOI:10.5194/cp-14-117-2018, 2018b.
- 891 Rasmussen, S. O., Vinther, B. M., Clausen, H. B., and Andersen, K. K.: Early Holocene climate
892 oscillations recorded in three Greenland ice cores, *Quaternary Sci. Rev.*, 26, 1907-1914,
893 DOI:10.1016/j.quascirev.2007.06.015, 2007.
- 894 Reche, I., Ortega-Retuerta, E., Romera, O., Villena, E. P., Baquero, R. M., and Casamayor, E. O.: Effect
895 of Saharan dust inputs on bacterial activity and community composition in Mediterranean lakes and
896 reservoirs, *Limnol. Oceanogr.*, 54, 869-879, DOI:10.4319/lo.2009.54.3.0869, 2009.

897 Reed, J. M., Stevenson, A. C., and Juggins, S.: A multi-proxy record of Holocene climatic change in
898 southwestern Spain: the Laguna de Medina, Cádiz, Holocene, 11, 707-719,
899 DOI:10.1191/09596830195735, 2001.

900 Reimer, P. J., Bard, E., Bayliss, A., Beck, J. W., Blackwell, P. G., Bronk Ramsey, C., Buck, C. E., Cheng,
901 H., Edwards, R. L., Friedrich, M., Grootes, P. M., Guilderson, T. P., Haflidason, H., Hajdas, I., Hatté, C.,
902 Heaton, T. J., Hoffmann, D. L., Hogg, A. G., Hughen, K. A., Kaiser, K. F., Kromer, B., Manning, S. W.,
903 Niu, M., Reimer, R. W., Richards, D. A., Scott, M., Southon, J. R., Staff, R. A., Turney, C. S. M., and van
904 der Plicht, J.: IntCal13 and Marine13 radiocarbon age calibration curves 0-50,000 years cal BP,
905 Radiocarbon, 55, 1869-1887, DOI:10.2458/azu_js_rc.55.16947, 2013.

906 Regattieri, E., Zanchetta, G., Drysdale, R. N., Isola, I., Hellstrom, J. C., Dallai, L.: Lateglacial to holocene
907 trace element record (Ba, Mg, Sr) from Corchia cave (Apuan Alps, central Italy): paleoenvironmental
908 implications, J. Quat. Sci., 29, 381-392, DOI:10.1002/jqs.2712, 2014.

909 Révillon, S., Jouet, G., Bayon, G., Rabineau, M., Dennielou, B., Hémond, C., and Berné, S.: The
910 provenance of sediments in the Gulf of Lions, western Mediterranean Sea, Geochem. Geophys. Geosy.,
911 12, Q08006, DOI:10.1029/2011GC003523, 2011.

912 Rodrigo-Gámiz, M., Martínez-Ruiz, F., Jiménez-Espejo, F. J., Gallego-Torres, D., Nieto-Moreno, V.,
913 Romero, O., Ariztegui, D.: Impact of climate variability in the western Mediterranean during the last
914 20,000 years: oceanic and atmospheric responses, Quaternary Sci. Rev., 30, 2018-2034,
915 DOI:10.1016/j.quascirev.2011.05.011, 2011.

916 Sawatzky, C. L., Wurtsbaugh, W. A., Luecke, C.: The spatial and temporal dynamics of deep chlorophyll
917 layers in high-mountain lakes: effects of nutrients, grazing, and herbivore recycling as growth
918 determinants, J. Plankton Res., 28, 65-86, DOI:10.1093/plankt/fbi101, 2006.

919 Schulte, L.: Climatic and human influence on river systems and glacier fluctuations in southeast Spain
920 since the Last Glacial Maximum, Quatern. Int., 93-94, 85-100, DOI:10.1016/S1040-6182(02)00008-3,
921 2002.

922 Sánchez-López, G., Hernández, A., Pla-Rabes, S., Trigo, R. M., Toro, M., Granados, I., Sáez, A.,
923 Masqué, P., Pueyo, J. J., Rubio-Inglés, M. J., and Giralt, S.: Climate reconstruction for the last two
924 millennia in central Iberia: The role of East Atlantic (EA), North Atlantic Oscillation (NAO) and their
925 interplay over the Iberian Peninsula, Quaternary Sci. Rev., 149, 135-150,
926 DOI:10.1016/j.quascirev.2016.07.021, 2016.

927 Settle D. M., and Patterson C. C.: Lead in Albacore: guide to lead pollution in Americans, Science, 207,
928 1167-76, DOI:10.1126/science.6986654, 1980.

929 Solanki, S. K., Usoskin, I. G., Kromer, B., Schüssler, M., and Beer, J.: Unusual activity of the Sun during
930 recent decades compared to the previous 11,000 years, Nature, 431, 1084-1087,
931 DOI:10.1038/nature02995, 2004.

932 Tjallingii, R., Röhl, U., Kölling, M., and Bickert, T.: Influence of the water content on X-ray fluorescence
933 core-scanning measurements in soft marine sediments, *Geoch. Geophys. Geosy.*, 8,
934 DOI:10.1029/2006GC001393, 2007.

935 Trigo, R. M., and Palutikof, J. P.: Precipitation scenarios over Iberia: a comparison between direct GCM
936 output and different downscaling techniques, *J. Climate*, 14, 4442-4446, DOI:10.1175/1520-
937 0442(2001)014<4422:PSOIAAC>2.0.CO;2, 2001.

938 Trigo, R. M., Pozo-Vázquez, D., Osborn, T. J., Castro-Díez, Y., Gámiz-Fortis, S., and Esteban-Parra, M.
939 J.: North Atlantic Oscillation influence on precipitation, river flow and water resources in the Iberian
940 Peninsula, *Int. J. Climatol.*, 24, 925-944, DOI:10.1002/joc.1048, 2004.

941 Trouet, V., Esper, J., Graham, N. E., Baker, A., Scourse, J. D., and Frank, D. C.: Persistent positive North
942 Atlantic Oscillation mode dominated the Medieval Climate Anomaly, *Science*, 324, 78-80,
943 DOI:10.1126/science.1166349, 2009.

944 Valbuena-Carabaña, M., López de Heredia, U., Fuentes-Utrilla, P., González-Doncel, I., and Gil, L.:
945 Historical and recent changes in the Spanish forests: a socioeconomic process, *Rev. Palaeobot. Palyno.*,
946 162, 492-506, DOI:10.1016/j.revpalbo.2009.11.003, 2010.

947 Valle, F.: Mapa de series de vegetación de Andalucía 1: 400 000, Editorial Rueda, Madrid, 2003.

948 Van der Weijden, C. H.: Pitfalls of normalization of marine geochemical data using a common divisor,
949 *Mar. Geol.*, 184, 167-187, DOI:10.1016/S0025-3227(01)00297-3, 2002.

950 Walczak, I. W., Baldini, J. U., Baldini, L. M., McDermott, F., Marsden, S., Standish, C. D., Richards, D.
951 A., Andreo, B., and Slater, J.: Reconstructing high-resolution climate using CT scanning of unsectioned
952 stalagmites: A case study identifying the mid-Holocene onset of the Mediterranean climate in southern
953 Iberia, *Quaternary Sci. Rev.*, 127, 117-128, DOI:10.1016/j.quascirev.2015.06.013, 2015.

954 Wanner, H., Brönnimann, S., Casty, C., Gyalistras, D., Luterbacher, J., Schmutz, C., Stephenson, D. B.,
955 and Xoplaki, E.: North Atlantic Oscillation—concepts and studies, *Surv. Geophys.*, 22, 321-381,
956 DOI:10.1023/A:1014217317898, 2001.

957 Wiersma, A. P., and Jongma, J. I.: A role for icebergs in the 8.2 ka climate event, *Climate dynamics*, 35,
958 535-549, DOI:10.1007/s00382-009-0645-1, 2010.

959 Wiersma, A. P., Roche, D. M., and Renssen, H.: Fingerprinting the 8.2 ka event climate response in a
960 coupled climate model, *J. Quat. Sci.*, 26, 118-127, DOI:10.1002/jqs.1439, 2011.

961 Yuan, F.: A multi-element sediment record of hydrological and environmental changes from Lake Erie
962 since 1800, *J. Paleolimnol.*, 58, 23-42, DOI:10.1007/s10933-017-9953-3, 2017.

963 Zanchetta, G., Drysdale, R. N., Hellstrom, J. C., Fallick, A. E., Isola, I., Gagan, M. K., Pareschi, M. T.:
964 Enhanced rainfall in the Western Mediterranean during deposition of sapropel S1: stalagmite evidence
965 from Corchia cave (Central Italy), *Quaternary Sci. Rev.*, 26, 279-286,
966 DOI:10.1016/j.quascirev.2006.12.003, 2007.

967

968 **List of tables**

<i>Lab Number</i>	<i>Depth (cm)</i>	<i>Dating Method</i>	<i>Age (14C yr BP±1σ)</i>	<i>Calibrated age (cal yr BP)2σ ranges</i>
	0	Present	2012 CE	-63
<i>Poz-72421</i>	7	14C	40±40	29-139
<i>D-AMS 008539</i>	22	14C	1112±32	935-1078
<i>D-AMS 008540</i>	39	14C	2675±30	2750-2809
<i>BETA-411994</i>	44	14C	3350±30	3550-3643
<i>BETA-411995</i>	55.5	14C	5480±30	6261-6318
<i>Poz-72423</i>	57.5	14C	5510±50	6266-6405
<i>Poz-72424</i>	62	14C	6450±50	7272-7433
<i>Poz-72425</i>	74	14C	8620±70	9479-9778

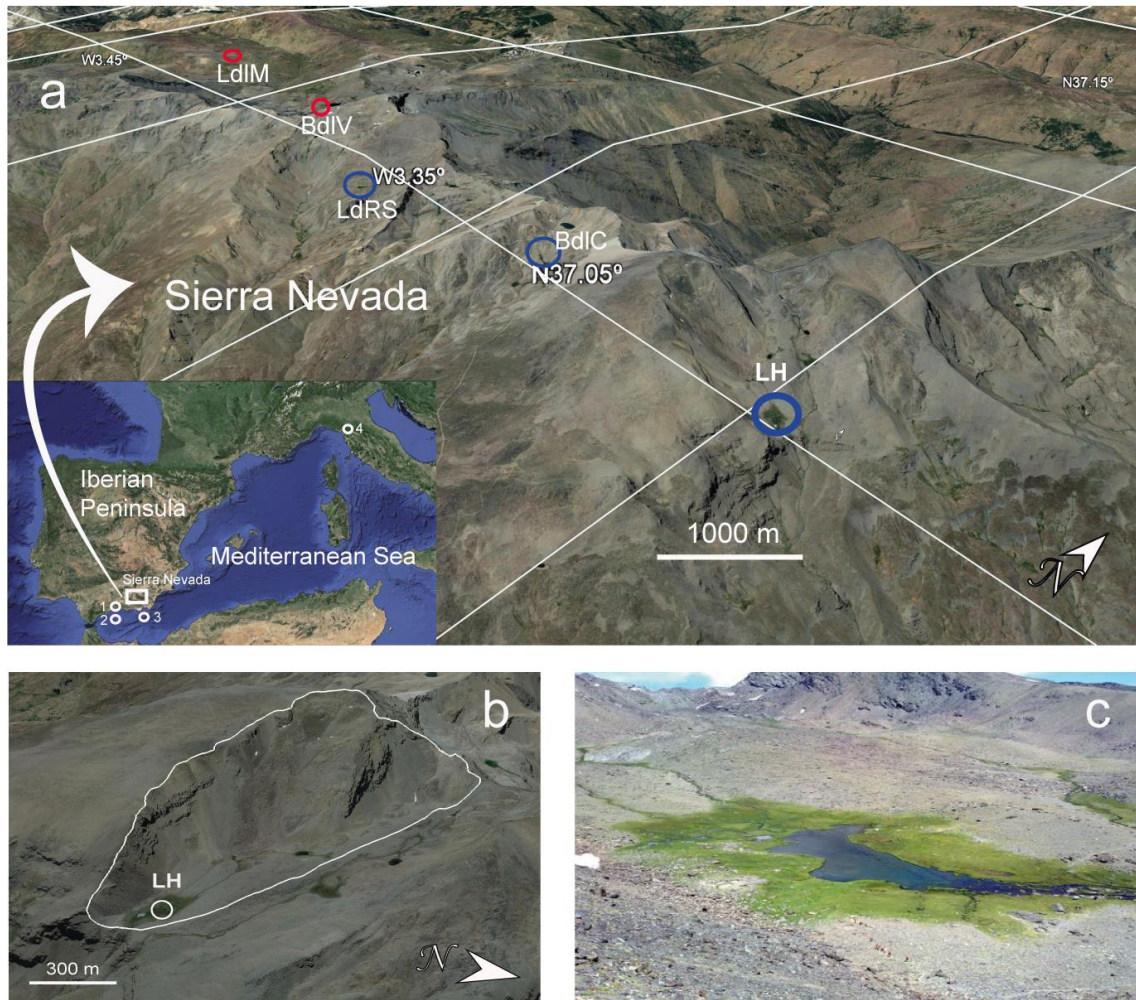
969 **Table 1.** Age data for LH 12-03 record. All ages were calibrated using IntCal13 curve (Reimer et al.,
 970 2013) with Clam program (Blaauw, 2010; version 2.2).

971
 972
 973
 974
 975
 976
 977
 978
 979
 980
 981
 982
 983
 984
 985
 986
 987
 988

	Simulation							
Correlation	A		B		C		D	
Ca/Ca (XRF)	0.63	p<0.01	0.50	p<0.01	0.57	p<0.01	0.54	p<0.01
K/K (XRF)	0.53	p<0.01	0.64	p<0.01	0.56	p<0.01	0.65	p<0.01

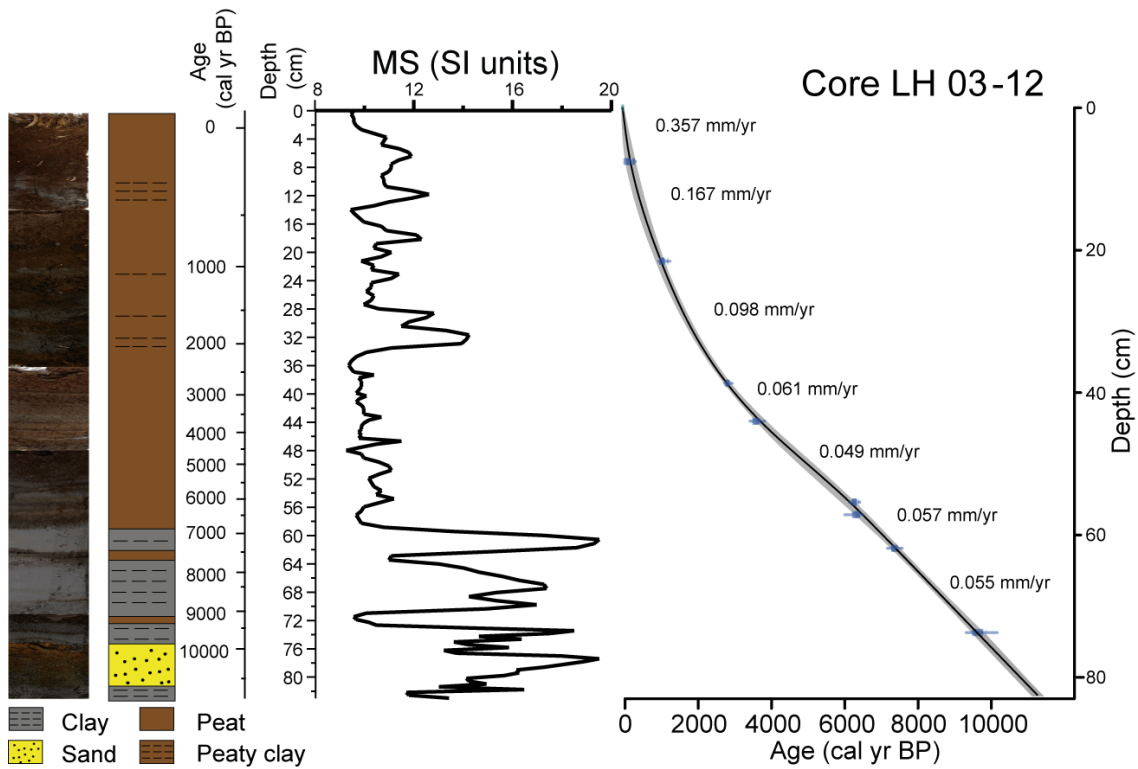
989 **Table 2.** Simulation of proxy correlation. A) regular interpolation of 300 years sampling spacing. B)
990 regular interpolation of 300 years sampling spacing and 5 data points moving average. C) regular
991 interpolation of 150 years sampling spacing. D) regular interpolation of 150 years sampling spacing and 5
992 data point moving average.

993
994
995
996
997
998
999
1000
1001
1002
1003
1004
1005
1006
1007
1008
1009
1010
1011
1012
1013
1014
1015
1016
1017
1018
1019
1020



1022

1023 **Figure 1.** (a) Location of the Laguna Hondera (LH) in Sierra Nevada, southern Iberian Peninsula, along
 1024 with other nearby records mentioned in the text. (1) El Refugio Cave stalagmite record (Walczak et al.,
 1025 2015); (2) ODP 976 pollen record (Combourieu-Nebout et al., 2009); (3) MD95-2043 pollen record
 1026 (Fletcher and Sánchez-Goñi, 2008); (4) CC26, Corchia Cave stalagmite record (Zanchetta et al., 2007;
 1027 Regattieri et al., 2014). Sierra Nevada north-facing sites are encircled in red, south-facing sites are
 1028 encircled in blue. LH: Laguna Hondera, the current study, is shown in bold. LdLM: Laguna de la Mula
 1029 (Jiménez-Moreno et al., 2013); BdLV: Borreguil de la Virgen (García-Alix et al., 2012; Jiménez-Moreno
 1030 and Anderson, 2012); LdRS: Laguna de Río Seco (Anderson et al., 2011; García-Alix et al., 2013;
 1031 Jiménez-Espejo et al., 2014); BdLC: Borreguil de la Caldera (Ramos-Román et al., 2016; García-Alix et
 1032 al., 2017) (b) Regional satellite photo of LH. The white line indicates the catchment area. (c) Photo of
 1033 Laguna Hondera in September 2012, when the core was taken. Photo taken by Gonzalo Jiménez-Moreno.
 1034 For the coloured figure, we refer the reader to the web version of this article.



1035

1036

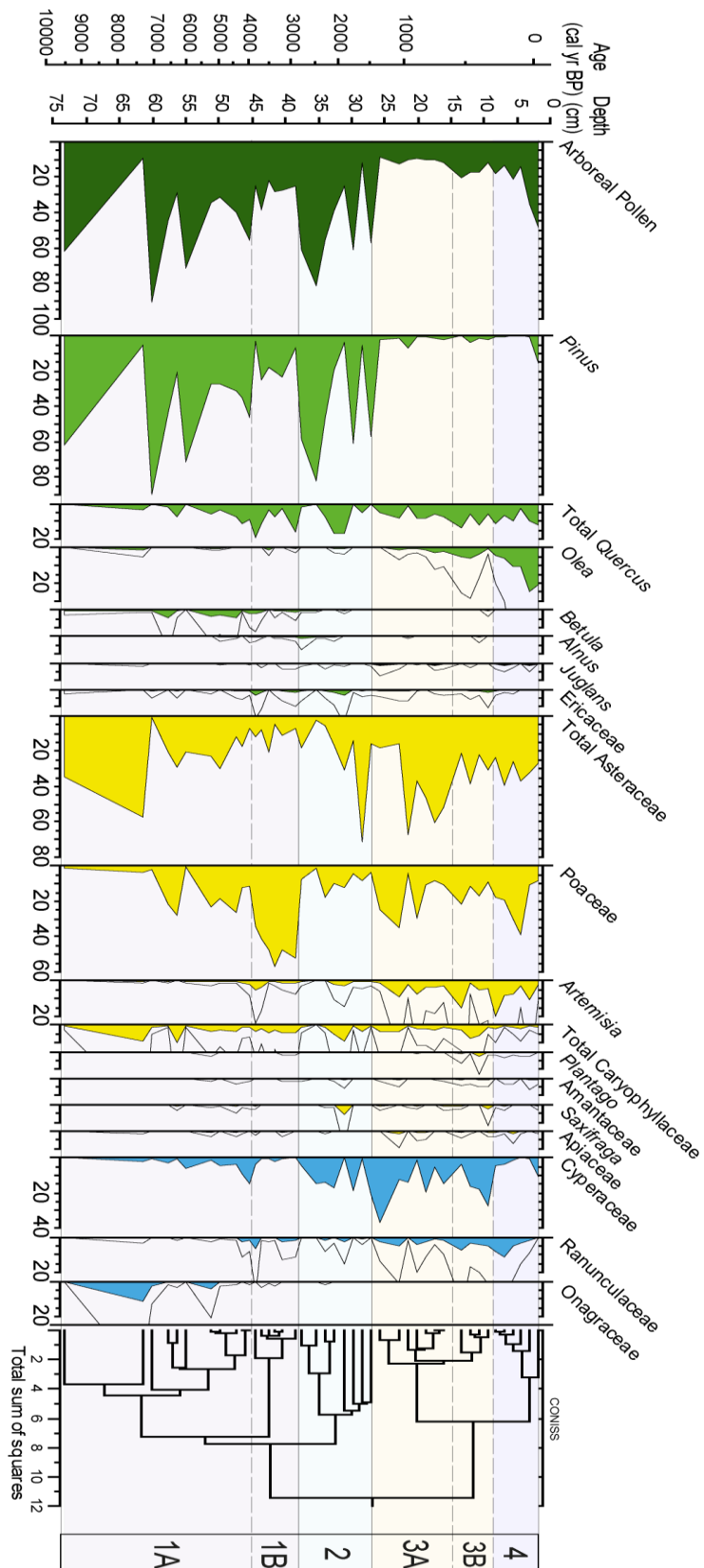
1037

1038

1039

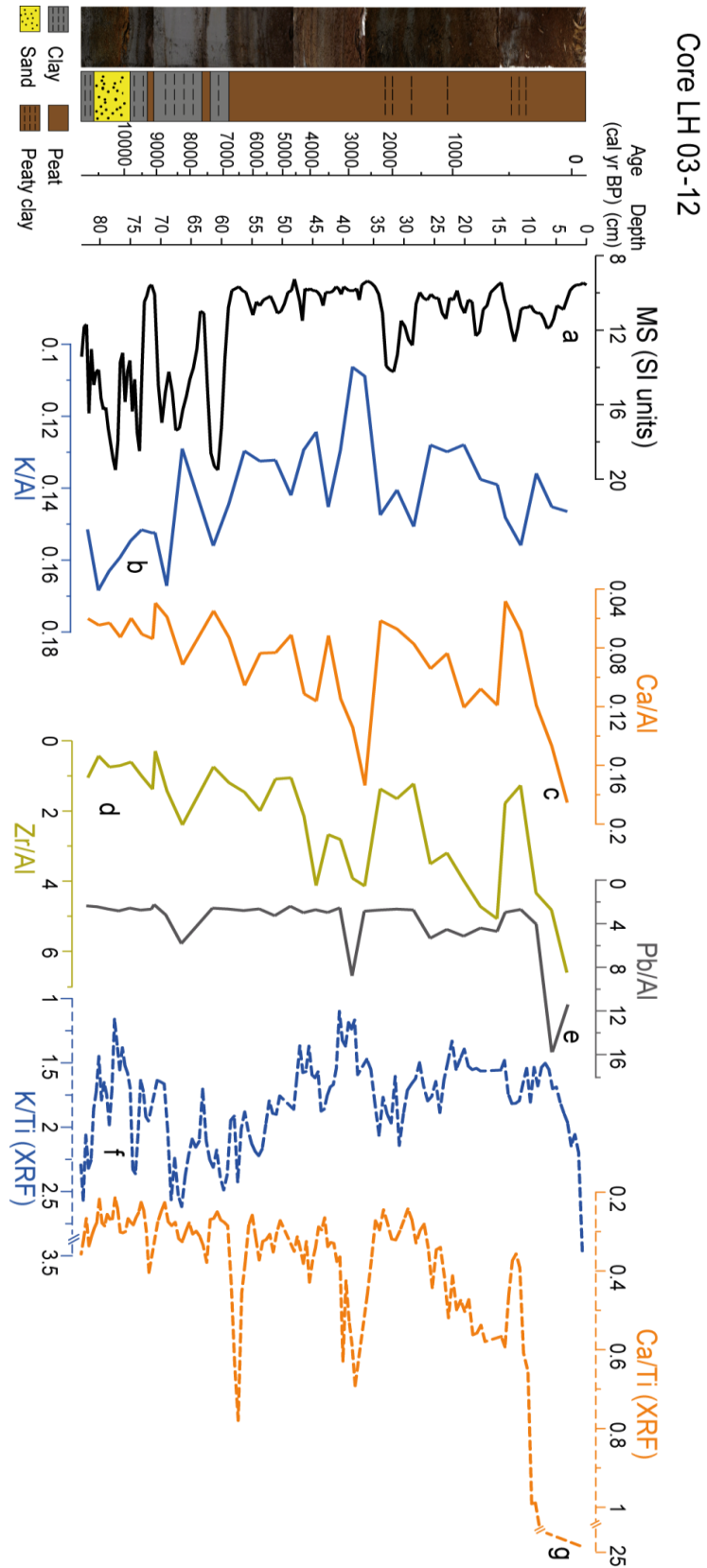
1040

Figure 2. Photo of core LH 12-03, along with the lithology, magnetic susceptibility (MS, in SI units) profile and age-depth model. Sediment accumulation rates (SAR in mm yr⁻¹) are shown between individual radiocarbon ages, the grey shadow represent the plus/minus range (see details in text for method of construction).



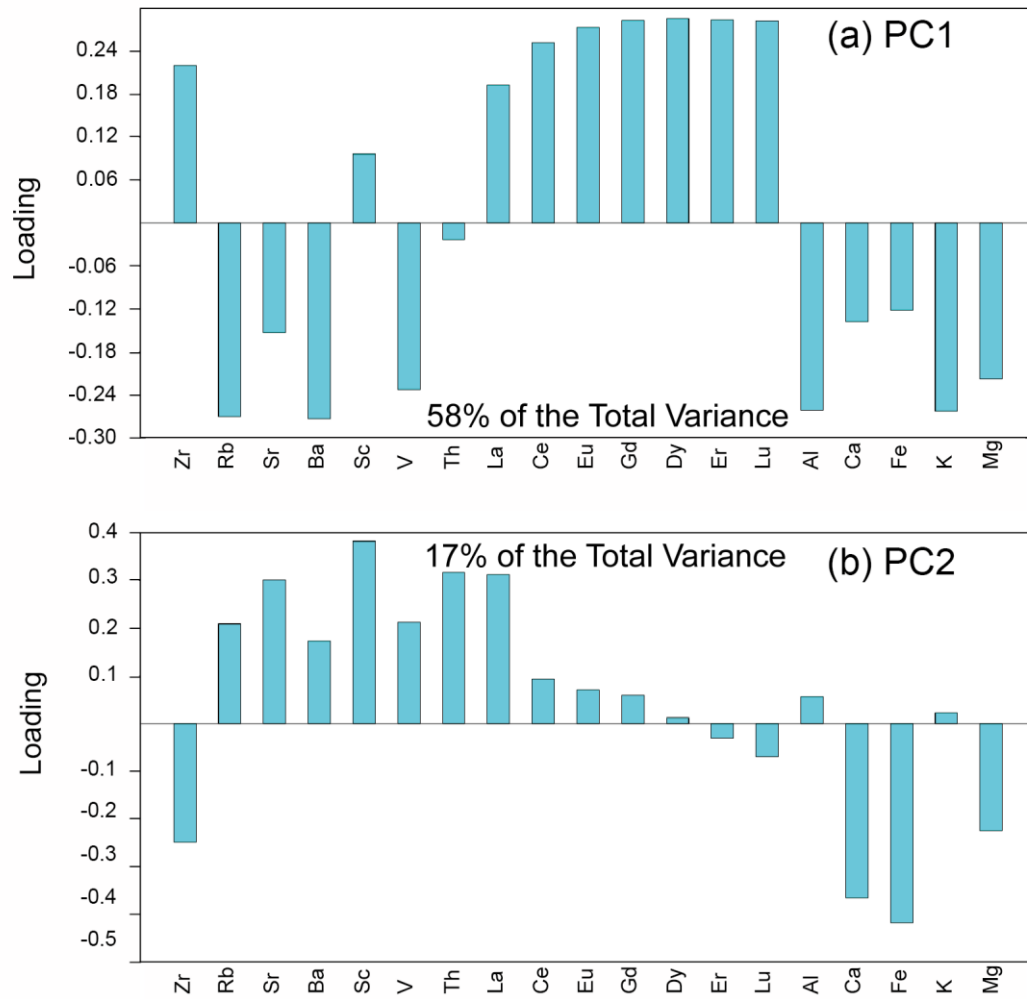
1041

1042 **Figure 3.** Pollen percentage diagram of the LH 12-03 record showing major selected taxa. Major tree
 1043 species are shown in green; shrubs and herbs are shown in yellow; and wetland and aquatic types are in
 1044 blue. Pollen was graphed with the Tilia software (Grimm, 1993), and zoned using the CONISS cluster
 1045 analysis program (Grimm, 1987).



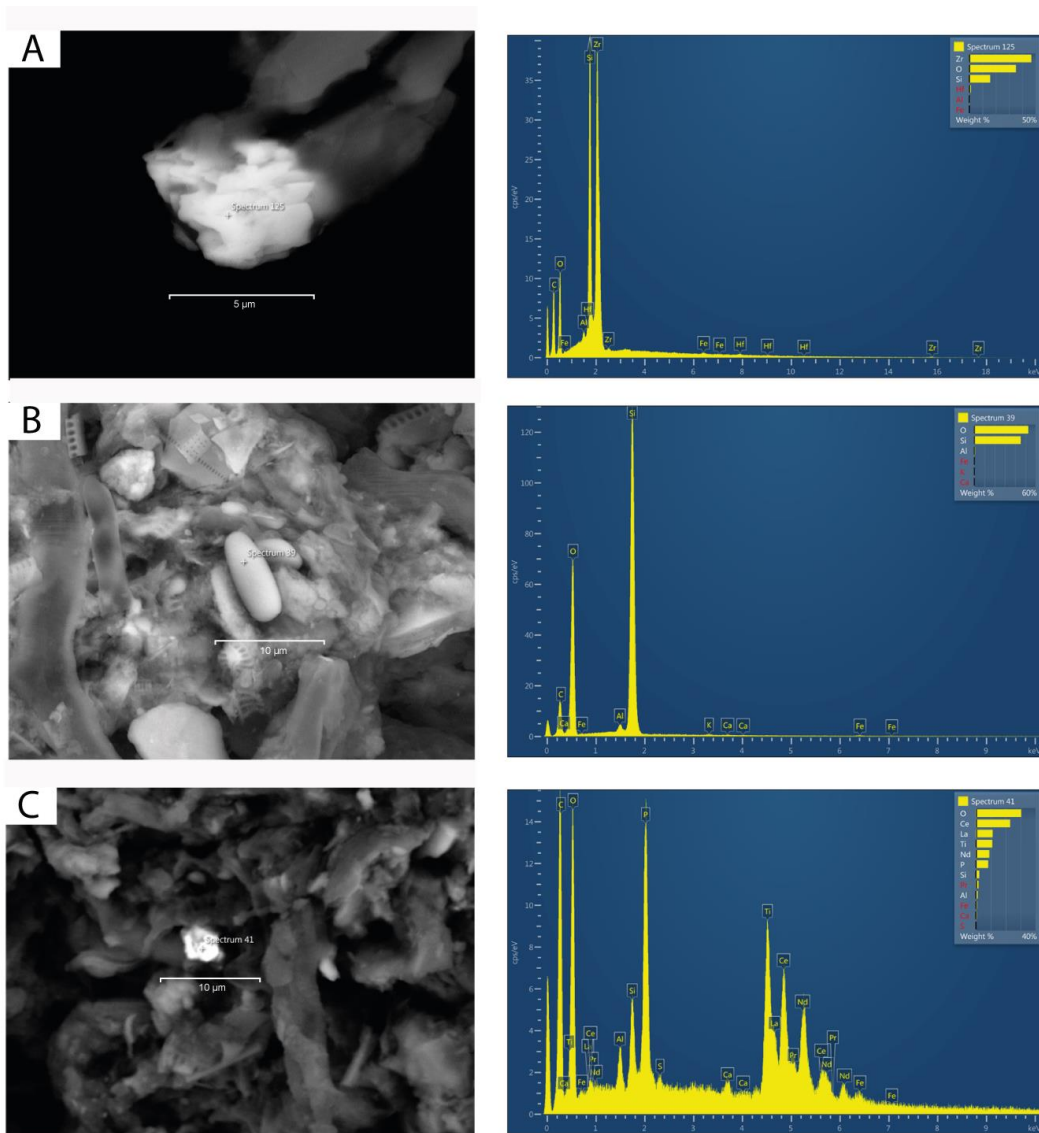
1046

1047 **Figure 4.** Detailed geochemical diagram of the LH 12-03 record showing the selected proxies: (a)
 1048 Magnetic Susceptibility (MS); (b) K/Al; (c) Ca/Al; (d) Zr/Al; (e) Pb/Al; (f) K/Ti (XRF); (g) Ca/Ti (XRF)
 1049 (MS in SI units, Zr/Al and Pb/Al scale $\times 10^{-4}$ and XRF in counts).



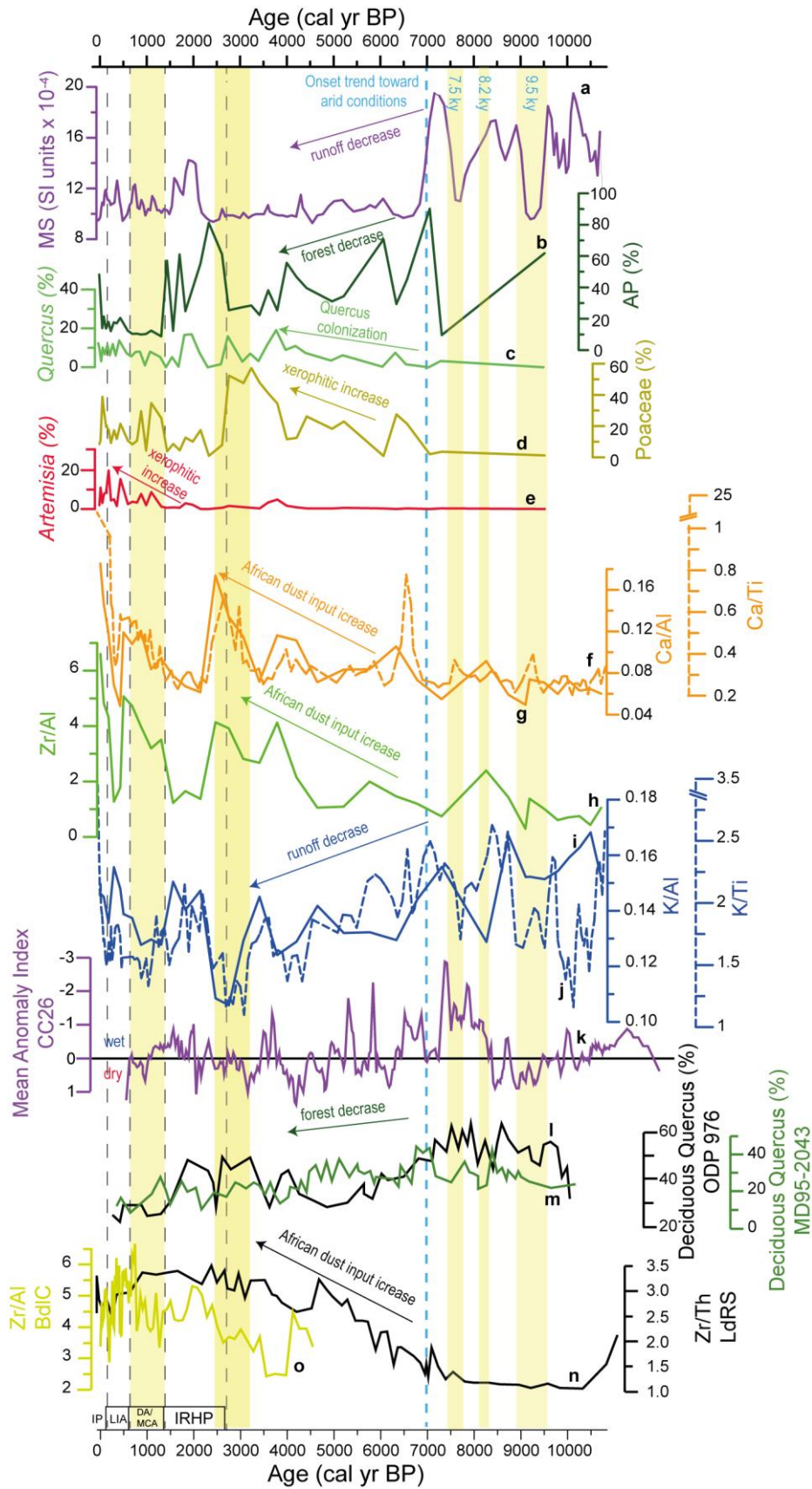
1050

1051 **Figure 5.** Principal Component Analysis (PCA) loadings from selected geochemical elements. (a) PC1,
 1052 which describes 58% of total variance; (b) PC2, which describes 17% of total variance.



1053

1054 **Figure 6.** Electron Backscatter Diffraction microphotographs of the LH 12-03 record with clearer colours
 1055 representing heavier minerals. (a) Zircon, with high Zr content; (b) rounded quartz related with eolian
 1056 transport; (c) monazite, with high REE content.



1057

1058 **Figure 7.** Comparison between the Magnetic Susceptibility (MS) data (in SI units $\times 10^{-4}$), the most
 1059 important pollen taxa and geochemical proxies from LH 12-03 record, with nearby paleoclimate records.
 1060 (a) MS from LH 12-03 record; (b) Arboreal Pollen (AP) percentage from LH 12-03 record; (c) *Quercus*

1061 percentage from LH 12-03 record; (d) Poaceae percentage from LH 12-03 record; (e) *Artemisia*
1062 percentage from LH 12-03 record; (f) Ca/Ti (XRF) ratio from LH 12-03 record in dashed line; (g) Ca/Al
1063 ratio from LH 12-03 record ; (h) Zr/Al ratio from LH 12-03 record; (i) K/Al ratio from LH 12-03 ; (j)
1064 K/Ti (XRF) ratio from LH 12-03 in dashed line; (k) Mean Anomaly Index from CC26 record (Corchia
1065 cave; Regattieri et al., 2014); (l) Deciduous *Quercus* from ODP 976 record (Alboran Sea; Combourieu-
1066 Nebout et al., 2009); (m) Deciduous *Quercus* from MD95-2043 record (Alboran Sea; Fletcher and
1067 Sanchez-Goñi, 2008); (n) Zr/Th ratio from Laguna de Río Seco (LdRS) (Jiménez-Espejo et al., 2014;
1068 García-Alix et al., 2018); (o) Zr/Al ratio from Borreguil de la Caldera (BdlC) (García-Alix et al., 2017;
1069 2018). Yellow bands indicate more arid intervals. Dark dashed lines are used for separating the different
1070 Current Era periods: IRHP: Iberian Roman Humid Period; DA: Dark Ages; MCA: Medieval Climate
1071 Anomaly; LIA: Little Ice Age; IP: Industrial Period. Blue dashed line indicates the onset of the trend
1072 toward arid conditions.

1073

1074

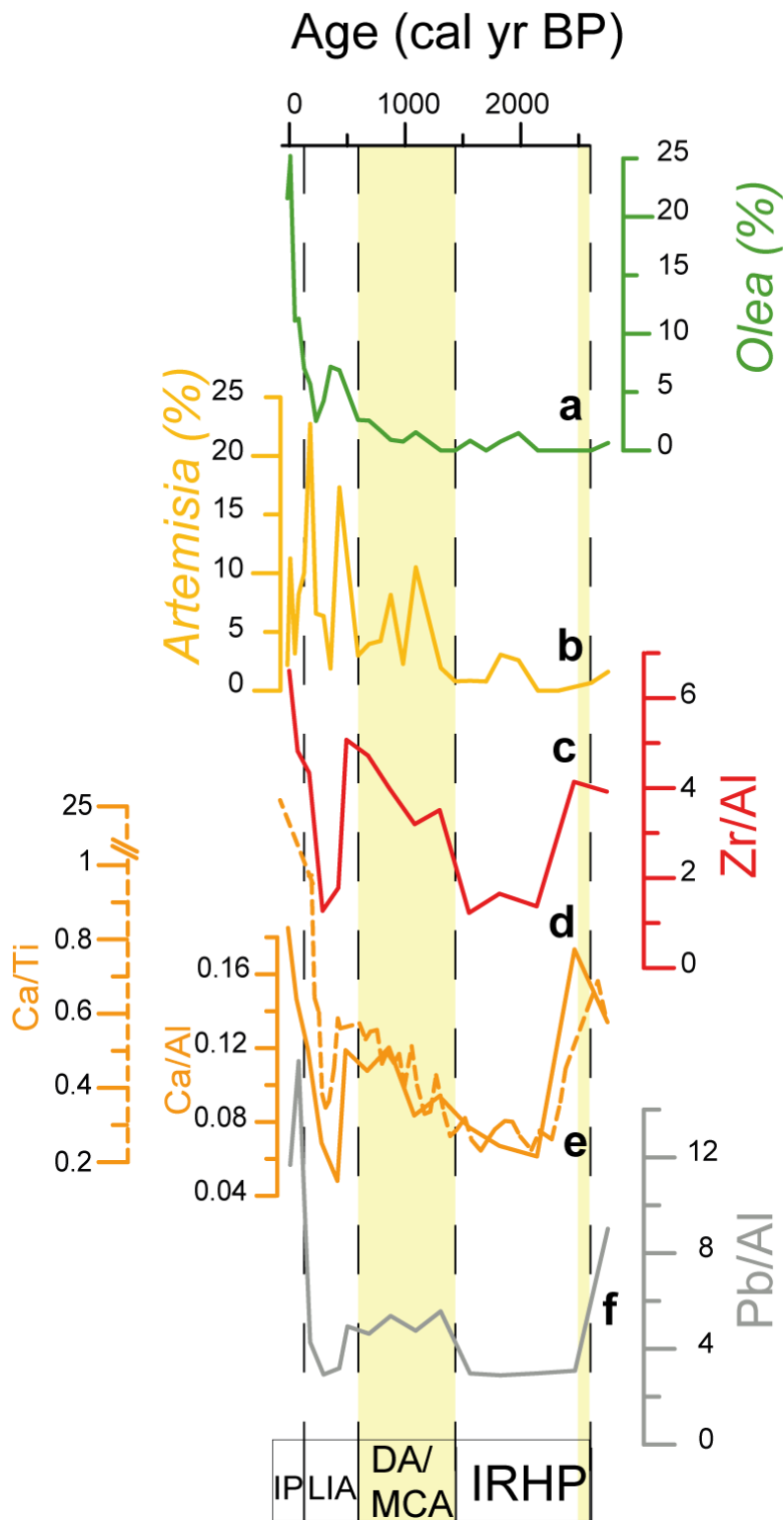
1075

1076

1077

1078

1079



1080

1081 **Figure 8.** Comparison of geochemical proxies with pollen taxa, related to anthropogenic impact for the
 1082 last ~2600 cal yr BP from LH 12-03 record. (a) *Olea* percentage from LH 12-03 record; (b) *Artemisia*
 1083 percentage from LH 12-03 record; (c) Zr/Al ratio from LH 12-03 record; (d) Ca/Al ratio from LH 12-03
 1084 record; (e) Ca/Ti (XRF) ratio from LH 12-03 record; (f) Pb/Al ratio from LH 12-03 record. Yellow bands
 1085 indicate more arid intervals. Dark dashed lines are used for separating the different Current Era periods:

1086 IRHP: Iberian Roman Humid Period; DA: Dark Ages; MCA: Medieval Climate Anomaly; LIA: Little Ice
1087 Age; IP: Industrial Period.